Drug Monitoring with Wearable Sweat Sensors

Li-Chia Tai

Electrical Engineering and Computer Sciences
University of California, Berkeley

Technical Report No. UCB/EECS-2022-11
http://www2.eecs.berkeley.edu/Pubs/TechRpts/2022/EECS-2022-11.html

May 1, 2022

Drug Monitoring with Wearable Sweat Sensors

By

Li-Chia Tai

A dissertation submitted in partial satisfaction of the

requirements for the degree of

Doctor of Philosophy

in

Engineering – Electrical Engineering and Computer Sciences

in the

Graduate Division

of the

University of California, Berkeley

Committee in charge:

Professor Ali Javey, Chair

Professor Ming-Chiang Wu

Professor Liwei Lin

Spring 2020

Abstract

Drug Monitoring with Wearable Sweat Sensors

By

Li-Chia Tai

Doctor of Philosophy in Electrical Engineering and Computer Sciences

University of California, Berkeley

Professor Ali Javey, Chair

Wearable sensors have been very popular among us to monitor our physical wellness, and they are potentially important for health monitoring with implications toward preventive care and clinical treatment. On the market, noninvasive wearables can be used to track external metrics such as heart rate and ECG signal. However, they fail to inform users about elusive biomarkers at the molecular level, which can potentially provide more insight into a person's health situation. Traditionally, accessing bio-molecular information requires collecting blood or urine samples with invasive extraction or logistic complications. In this regard, sweat stands out as a great candidate because of its noninvasive property and abundance in biomolecules, such as electrolytes, metabolites, xenobiotic molecules, and heavy metals. Our group has demonstrated noninvasive and multiplexed sensing of biomolecules by interfacing flexible printed circuit boards and electrode arrays. The advantage of this kind of sensor is that it enables real-time monitoring, requires small sample volume, and detects multiple biomolecules simultaneously. The sweat monitoring device allows us to potentially monitor our health statuses and screen diseases. However, a challenge that is equally important to screening diseases is to have an effective treatment that typically involves drug intake. So the question that remains is whether we can monitor drug molecules using a wearable sweat sensor?

After an introduction in Chapter 1, we will explore this possibility in Chapter 2. A methylxanthine drug, caffeine, is selected to validate the sensor's functionalities. Chapter 3 seeks the sensor's potential applications in clinical settings. The focus is on levodopa, which is typically used for treating patients with Parkinson's disease. In Chapter 4, the sensing platform is reconfigured for secondhand smoke detection, which can potentially be used by a broader population. In summary, we have demonstrated wearable sweat sensors capable of monitoring selected molecules related to drugs. This work leverages a wearable sweat sensor towards noninvasive and continuous point-of-care drug monitoring and management.

To my family, church, and friends

Acknowledgments

I vividly recall the day when I first arrived at UC Berkeley, a chilly day on July 20th of 2015. I had traveled to the US with my younger sister, and the long journey and the cold wind in the Berkeley Hills had caused me to shiver and miss my hometown – a warm subtropical island.

Thankfully, I was quickly greeted by members of the Javey Lab. Professor Javey invited me to his office and told me that a Ph.D. would be a long journey. "Be patient. I guarantee that you will get there if you are persistent and patient." That was the first advice he gave me, and it had proven to be very true. As a world-famous researcher, Professor Javey's strong and visionary insights for research had motivated me to pursue excellence, integrity, and truth. On a personal level, he always made himself available to discuss projects and made sure that I was on track toward finishing a Ph.D. I am grateful for his careful guidance over the past five years. His encouragement during various hills and valleys of my life will be greatly missed.

I would like to thank all the Javey Lab members, past and present. Professor Wei Gao, Professor Hiroki Ota, Professor Sam Emaminejad, Professor Daisuke Kiriya, Dr. Hossain Fahad, and Dr. Der-Hsien Lien guided me through many years of research. I am grateful for the company of the sensor subgroup. Hnin Yin Yin Nyein, Mallika Bariya, Dr. Yuanjing Lin, Serena Blacklow, Dr. Lu Li, Jiangqi Zhao, Lei Hou, Zhen Yuan, and Brandon Tran have been great companions in the lab. My mentees, Minghan Chao, Quynh Ngo, Ziba Shahpar, Eric Wu, Tiffany Sun Liaw, and Christine Heera Ahn have played critical roles. I thank my collaborators, Professor Gyoujin Cho and Professor Zhiyong Fan, whom I worked with closely for the caffeine and levodopa projects. I also give my gratitude to other members of the Javey Lab who have provided me guidance, feedback, and support. Because of all of them, I was able to be involved in various projects related to biomedical sensors and became excited about medicine. Without them, I would not have been able to go through this long journey with much joy and laughter.

The committee members of my Ph.D. preliminary exam and qualifying exam played essential roles in shaping my research career. The preliminary exam took place on August 22, 2016. Three committee members were Professor Ming-Chiang Wu, Professor Constance Chang-Hasnain, and Professor Eli Yablonovitch. The qualifying exam took place on October 25, 2017. The committee members were Professor Ali Javey, Professor Ming-Chiang Wu, Professor Liwei Lin, and

Professor Dorian Liepmann. All of them had helped me solidify my research foundations and directions significantly. Three of them are now serving on my thesis committee. I am also thankful for my classmates and friends in my department. Yen-Kai Lin, Wen Chuen Liu, and Guo-Lun Luo have been great encouragements to me during my time at Berkeley. I want to thank my funding sources, including the National Science Foundation (NSF) Nanomanufacturing Systems for Mobile Computing and Mobile Energy Technologies (NASCENT), the Berkeley Sensor & Actuator Center (BSAC), and the Electronic Materials (E-MAT) laboratory funded by the Director, Office of Science, Office of Basic Energy Sciences, Material Sciences and Engineering Division of the U.S. Department of Energy under Contract No. DE-AC02-05CH11231.

My friends at UCLA – I remember you. Professor Bahram Jalali, Dr. Ata Mahjoubfar, Dr. Claire Chen, Professor Keisuke Goda, Professor Chao Wang, and Nora Brackbill had mentored me significantly during my time in the Jalali Lab. Paul Chin, Winson Huang, Cheng-Yi Lin, and Albert Hsu have been encouraging friends and classmates. Henry Lin and Roanna Cheung, Professor Frank Chang, and friends from Tree of Life fellowship prayed for me during the time when I was lost. Without all of you, I would not have enjoyed college so much and made it to Berkeley for graduate school. I thank my alma mater, UCLA, for teaching me to be humble and brave.

I had wonderful teachers even before I started college. Mrs. Liu, Mrs. Huang, and Mrs. Chen from Dongguang Elementary School taught me to be disciplined. Mrs. Tsao from Yang Ming Junior High School and Mr. Gan from Kaohsiung Senior High School motivated me to study hard and encouraged me to become a scientist. I am grateful for their countless hours of mentorships. I also want to thank Mr. Simon and Ms. McCallum for being my English teachers.

I want to give my gratitude to my church family from the International Graduate Student Ministry (IGSM) and Gracepoint Church. Pastor Edward Kang and Kelly Kang, Tony Sun and Michelle Sun, Chul Kim and Sharon Kim, Jisup Hong and Sara Hong, Paul Chen and Mary Chen, Jim Kwak and Julie Kwak, Shufei Lei and Karen Lei, Hank Xu and Joy Xu, Kig Ng and Connie Ng, Mark Borja and Grace Borja, Howard Lei and Pacie Lei, Peter Kim and Lynda Kim, Caleb Chung and Jenny Chung, Bo Zheng and Kuan Zheng, and Kevin Limkrailassiri and Jean Limkrailassiri are couples who have helped me grow in my faith and overcome challenges in life. My previous and current housemates, Bing Zhang, Khetpakorn Chakarawet, Brian Phegley, Eric Ge, Spencer Lyu, Yu-Chieh Eddy Lan, Jaeyeon Ahn, Unpil Baek, Sean Hong, Raymond Iu, Ken Ikawa,

Kazuya Tsuge, Jiwon Son, Samuel Lee, Dai Wang, Jonathan Eng, Larry Tan, Paul Jung, Yubo Diwu, Naing Ye Aung, Edwin Xiong, and Jerry Hu have shared many exciting as well as sorrowful moments with me. Other people who have labored and prayed with me in ministry include Jeff Chiu, Chenghui Yu and Judy Yu, Hanzen Lim, Gary Zhao and Summer Zhao, Bryan Zheng and Jilan Zheng, Peter Wang and Stephanie Wang, and Adam Kor. Other long-time friends in IGSM who have accompanied me through the Ph.D. journey include Josh Yeung, Daniel Liu, Jeff Chan, Nghia Tran and Elaine Tran, Charlie Yeh, Yuxun Zhou, Jon Gonzales, Josh Chin, Yue Fu, Cheng Ding, Wesley Wu, Lei Meng, Mingdian Tan, Sean Liu, Yimin Li, Yi-Chuan Lu, Jacklyn Ang, Eliana Huangfu, Jenny Huang, Wenxia Lin, and Hanna Hou. They are the pillars that have been supporting me through the ups and downs of graduate school.

I would like to thank my parents for raising me and always being there. I can always rely on you. Even though you have busy work schedules, sometimes with evening shifts and long hours of surgeries to operate, you always make sure that we have everything we need for school. To my mom, I want to thank you for always cooking for us after work. Whenever I face difficulty and frustration in life, you are always there to support me and redirect me to look to the bright side. To my dad, thank you for bringing us on family trips and always initiating conversations with us. I always get a lot of inspiration and research ideas from you. To my younger sisters, I remember the various games we played together when we were young. The stuffed animals in our wardrobes were the best memories of my childhood. They remind me to be daring in dreaming big dreams. To my first younger sister, I am happy to see you finishing your training to become a doctor and fulfilling your dream to volunteer in Africa. To my second younger sister, I hope you will enjoy the rest of your college and make your way to graduate school in the US. To my grandparents, I want to thank you for loving me and being patient when I can barely visit you in Taiwan. To my aunt and uncle in Los Angeles, I am thankful for the kind of care I received from you when I first started college at UCLA. The words cannot express my gratitude to all of you. For those of you whom I haven't mentioned, I know that you are there supporting me, and I am deeply grateful for your presence.

I thank God and Jesus Christ for being my shepherd. Without your love, mercy, and forgiveness, I will not be able to stand various trials in life and experience great joy from knowing that you always have better plans beyond my imagination. One of my favorite verses from Jeremiah 29:11: "For I know the plans I have for you, declares the LORD, plans for welfare and not for evil, to give you a future and a hope." Even in the valleys of my life, you are a shield about me,

my refuge, and my fortress (Psalm 3 and Psalm 91). In various chapters of my life, you always remind me of Thessalonians 5:16-18: “Rejoice always, pray without ceasing, give thanks in all circumstances; for this is the will of God in Christ Jesus for you.” These verses have been a great source of my strength. Because of you, I am able to relate with my brothers and sisters in Christ with generosity, love, and prayer. I am indebted to them for many prayers. It is my prayer that the gospel may shine through this dedicated work, which is a testimony to your sovereignty in this world.

The weather has become warm on this subtropical island. The global pandemic has brought many people home. In hindsight, I won’t say that going through a Ph.D. program is chill, but I have no regrets because of so many wonderful stories made possible through my time at Berkeley. Looking out of the window, I long to see all of you there in Berkeley, that I may be filled with joy. The wind is good – it’s perhaps time to set sail.

Li-Chia Jerry Tai

May 12, 2020

Kaohsiung, Taiwan
& Berkeley, CA, USA

Table of Contents

Chapter 1 Introduction

1.1 Need for wearable drug monitoring sensors

Drug monitoring plays crucial roles in doping control and precision medicine. It helps physicians tailor drug dosage for optimal benefits, track patients' compliance to prescriptions and understand the complex pharmacokinetics of drugs. Conventional drug tests rely on invasive blood draws. While urine and sweat are attractive alternative biofluids, the state-of-the-art methods require separate sample collection and processing steps and fail to provide real-time information. Here we present a wearable platform equipped with an electrochemical differential pulse voltammetry (DPV) sensing module for drug monitoring. A methylxanthine drug, caffeine, is selected to demonstrate the platform's functionalities. Sweat caffeine levels are monitored under various conditions, such as drug doses and measurement time after drug intake. Elevated sweat caffeine levels upon increasing dosage and confirmable caffeine physiological trends are observed. Our work leverages a wearable sweat sensing platform towards noninvasive and continuous point-of-care drug monitoring and management.

1.2 Toward clinical applications with drug monitoring sensors

After developing a wearable platform for drug monitoring, we seek potential applications of the sensor in clinical settings. The molecule of our choice, levodopa, which is the standard medication clinically prescribed to patients afflicted with Parkinson's disease. In particular, the monitoring and optimization of levodopa dosage is critical to mitigate the onset of undesired fluctuations in the patients' physical and emotional conditions, such as speech function, motor behavior and mood stability. The traditional approach to optimize levodopa dosage involves evaluating the subjects' motor function, which has many shortcomings due to its subjective and limited quantifiable nature. Here, we present a wearable sweat band on a nano-dendritic platform that quantitatively monitors levodopa dynamics in the body. Both stationary iontophoretic induction and physical exercise are utilized as our methods of sweat extraction. The sweat band measures real-time pharmacokinetic profiles of levodopa to track the dynamic response of the drug metabolism. We demonstrated the sweat band's functionalities on multiple subjects with implications towards the systematic administering of levodopa and routine management of Parkinson's disease.

1.3 Drug monitoring sensors for the general public

After demonstrating the wearable sensor's application in practical settings, we aim to reconfigure the platform for use by a broader population. The application of our choice is related to the tobacco epidemic, which is a public health threat that has taken a heavy toll of lives around the globe each year. Smoking affects both the smokers and those who are exposed to secondhand smoke, and careful tracking of exposure can be key to mitigating the potential hazards. For smokers, the variation of chemical compositions between commercial cigarettes has led to ambiguity in estimating the health risks, both for active smokers and others involuntarily exposed to tobacco smoke and byproducts. In this regard, sweat possesses an attractive opportunity to monitor smoke exposure due to sweat's abundance in biomolecules and its great accessibility. Here we present a wearable sweat band to monitor nicotine, a prominent ingredient in cigarettes, as a viable way to quantitatively assess a wearer's exposure to smoking. Both smokers and normal subjects are tested to demonstrate the use of this device for smoke-related health monitoring. Our results exhibit confirmable, elevated nicotine levels in sweat for subjects inhaling cigarette smoke. This continuous and personalized sweat sensing device is leverage to monitor smoke pollution for a potentially broad population.

Chapter 2 Caffeine Monitoring with Wearable Sweat Sensors

The following chapter has been previously published in a similar format.

2.1 Introduction to Caffeine Monitoring

Drug analysis is the chemical testing of human biological samples to determine the subject's drug history. It is commonly implemented for doping control, drug abuse testing, forensic investigation, clinical therapeutics and digital health monitoring.[1-3] Sources of biological specimens for drug analysis include blood, urine, saliva, hair, sweat and exhaled breath.[4-10] Conventional blood analysis provides the most direct and accurate approach to track drug dosage, but it is an invasive technique with limited sample collection. Recently, *in-situ* sweat analysis is quickly becoming an attractive alternative in noninvasive diagnosis.[11,12] The distinct nature of secretion, accessibility and abundance in biomolecules make human sweat an ideal candidate for point-of-care health monitoring.[11-14]

Recent advances in wearable biosensors have made great strides in providing non-obstructive and on-site analysis of human health conditions.[14-32] A sensitive and selective approach to multiplexed sensing of sweat biomolecules can be achieved by utilizing wearable electrochemical sensors.[14,19,21] Such sensors usually consist of flexible sensors for signal transduction coupled with electrical circuit components for signal conditioning and data transmission. This platform provides users with valuable physiological insight into their states of health. Previously reported wearable sweat sensors are capable of monitoring electrolytes and metabolites (sodium, potassium, glucose, lactate, etc) for health monitoring and disease diagnosis via traditional techniques such as amperometry, potentiometry, colorimetry, etc.[19-27] However, designing wearable sweat sensors capable of retrieving information regarding drug intake, which is important for disease treatment, remains to be an obstacle. The detection of drug molecules is challenging owing to their ultra low concentrations in biofluids, and it usually requires very different detection mechanisms. As an example, the differential pulse voltammetry (DPV) is commonly employed to detect drug molecules. The mechanism is based on oxidation of the target molecule at its distinct oxidation

potential. The corresponding current flow is then measured with an undesirable capacitive component eliminated to allow sensitive determination of the molecule's concentration.[33-36] The oxidation potential involved in the DPV detection can be relatively high, so stringent requirements on electrode stability to retain sensor integrity at high operating potential are necessary.[35,36] Thus, a sensible strategy to design wearable drug sensors is to combine high potential resilient electrochemical sensors and integrated circuitry devised with DPV implementation. Specifically, this can be achieved by consolidating large scale and low cost printed carbon electrodes and printed circuit boards.

Here we present a wearable sweat band (*s*-band) for noninvasive and *in-situ* monitoring of drug levels. In this work, caffeine is selected as an example methylxanthine drug to demonstrate the sensor's functionalities. Caffeine is a relatively safe drug and widely dosed through coffee, tea and other related commercial products. Clinically, its chronic overdose can potentially lead to health problems such as coronary syndromes, hypertension and depression.[37-39] It is also an ergogenic drug restricted in official athletic competitions, which often require standard assessment of urine caffeine prior to tournaments.[40] It has been reported that urine caffeine concentration correlates with both plasma and sweat caffeine concentrations.[41,42] Thus, monitoring sweat caffeine would effectively provide us with insight into caffeine levels. More importantly, the DPV detection technique for caffeine is fundamentally similar to those used for many other types of drugs,[33-35] so we envision that this sensor platform can be exploited towards detection of a number of other drugs. In this work, caffeine detection is successfully performed in collected human sweat samples as well as on-body to investigate the influence of caffeine dosage upon sweat caffeine levels using the *s*-band platform. This platform resolves the technological challenge of wearable sweat sensors for drug monitoring and can serve as a powerful tool that paves the way for continuous and noninvasive drug monitoring.

2.2 Device Background and Sensing Mechanism

Figure 1a illustrates the wearable platform packaged into a wristband for on-body sweat analysis. The platform consists of a triple-electrode array patterned on a flexible polyethylene terephthalate (PET) substrate and interfaced with a printed circuit board (PCB). Figure 1b shows the schematic of the printed electrodes used for electrochemical sensing: a carbon working electrode (WE) modified with carbon nanotubes (CNTs)/Nafion films, a carbon counter electrode (CE) and a Ag/AgCl reference electrode (RE). The choice of working electrode material critically determines the types of chemical reactions permitted on the electrode

surface. Carbon is favorably selected due to its stability under high sweeping voltage for drug detection, as well as its low cost and biocompatibility to human skin.[36] Roll-to-roll printing technology is exploited to produce high performance electrode arrays at large scale. At the system level, as shown in Figure 1c, the completely integrated *s*-band includes signal transduction, conditioning, processing and Bluetooth transmission functionalities to relay electrochemical signals to a user interface and allow *in-situ* monitoring of drug levels. Figure 1d illustrates the electrochemical caffeine detection mechanism that underlies the technology: the implementation of DPV from the PCB and the oxidization of caffeine molecules at around 1.4 V. The electrical current level detected at the oxidation peak provides a quantitative measurement of sweat caffeine concentration. After drug intake, sweat can be accessed via vigorous physical exercise or iontophoresis and analyzed by the *s*-band, as shown in Figure 1e and detailed in the Experimental Section.

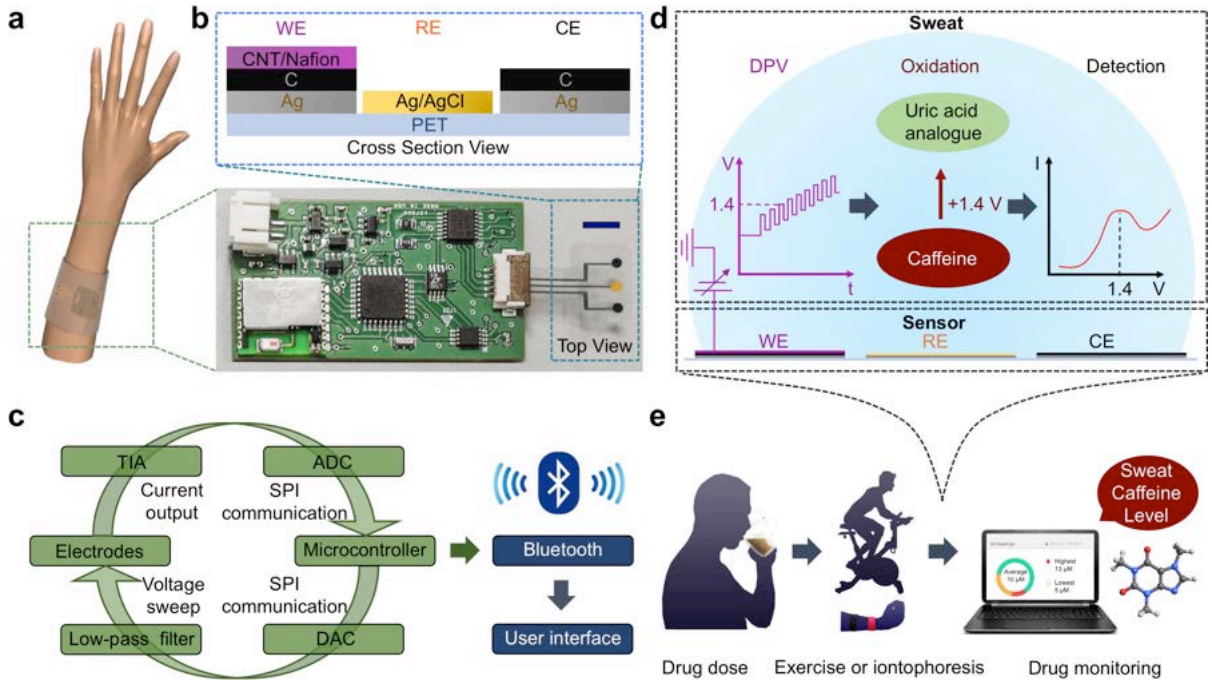

Figure 1. Schematic of the *s*-band and drug sensing mechanism. a) Schematic of the *s*-band worn on a subject's wrist. b) Optical image of the *s*-band and the cross-section view of a roll-to-roll printed flexible sensor patch. Scale bar, 5 mm. WE, RE and CE are working electrode, reference electrode and counter electrode. c) System-level diagram of the *s*-band platform for real-time sensing, data processing and wireless transmission. d) Electrochemical detection of caffeine through differential pulse voltammetry (DPV). Oxidation of caffeine leads to an observable oxidation peak around 1.4 V. e) Real-time sweat caffeine monitoring using the *s*-band after caffeine intake. (Reprinted with permission from John Wiley and Sons).

2.3 Sensor Characterization

The flexible electrodes were prepared through the roll-to-roll printing process.[43] The carbon working electrode was modified with CNTs/Nafion films through drop casting (detailed in the Experimental Section). This step is crucial for anti-fouling protection of the sensing electrodes in sweat samples and improves the sensor's detection limit.[20,44]

The caffeine sensor is characterized electrochemically using DPV in a solution containing different caffeine concentrations. Figure 2a shows the DPV response of the sensor in 0-40 µM caffeine solution (dissolved in 0.01 M acetate buffer to simulate human sweat).[20,21] The voltammetry range of 1.1 V to 1.7 V is selected to cover the oxidation potential of caffeine.[36] The current peak can be

measured according to a standard technique described in Figure S1 (Supporting Information). Figure 2b shows an extracted linear relationship of the sensor's responses to the caffeine concentrations with a high sensitivity of 110 nA μM^{-1}.

Sweat normally contains a wide variety of chemicals that can potentially interfere with the sensors' performance.[20-23] Hence, the selectivity of the *s*-band sensor is evaluated in Figure 2c to ensure the fidelity of the sensor readings under practical conditions. Since the *s*-band platform relies on oxidation reactions to detect caffeine, major sweat biomolecules that can be oxidized are chosen for the selectivity test. Specifically, urea (30 µM), glucose (100 µM), lactic acid (10 mM), ascorbic acid (10 µM) are added to the caffeine solution with physiologically relevant concentrations.[14,23] In addition, pilocarpine (15 mM), which is commonly used to induce sweat, is added in the selectivity test.[19] The results show that the change in sensor response due to potential interferents falls within 9.2%.

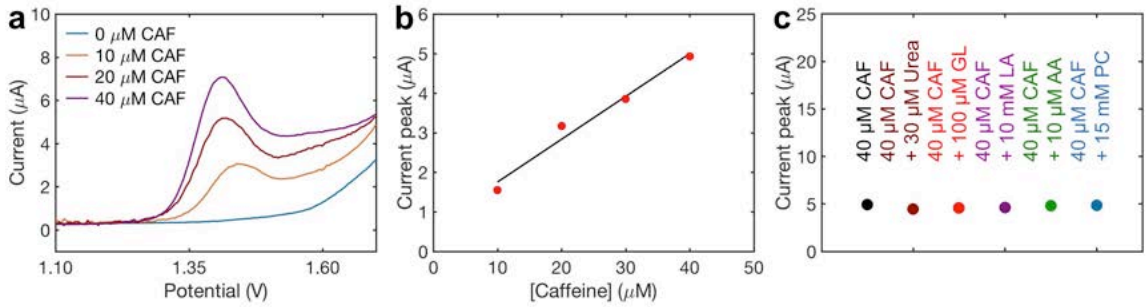

Figure 2. Characterization of the caffeine sensor based on roll-to-roll printed CNTs/Nafion modified carbon electrodes. a) Differential pulse voltammograms (DPV) of caffeine (0-40 µM) dissolved in a 0.01 M acetate buffer solution (pH 4.6) and b) the corresponding calibration curves. c) Interference studies of the caffeine sensor. In each subsequent DPV measurement, 30 µM urea, 100 µM glucose (GL), 10 mM lactic acid (LA), 10 µM ascorbic acid (AA), or 15 mM pilocarpine (PC) is added to a 40 µM caffeine (CAF) solution. (Reprinted with permission from John Wiley and Sons).

2.4 Iontophoresis and Exercise Experiments

In order to demonstrate the functionalities of the sensor platform, two healthy subjects were selected for caffeine dose trials. Prior to an experiment, each subject is required to abstain from caffeine intake overnight. At the beginning of the trial, the subject either consumes a single-shot or triple-shot espresso coffee (~75 mg or ~225 mg caffeine).[45] In the controlled experiment, the subject does not

consume any coffee. The subject then waits for half an hour in resting mode. Afterwards, the subject's wrist is cleaned with alcohol wipe and loaded with a cholinergic agonist hydrogel to perform iontophoresis (sweat inducing technique). Following an iontophoresis procedure in a previous report,[19] a 5-minute 1-mA electrical current is applied to drive sweat-inducing pilocarpine drug, entrapped in a hydrogel, into the sub-dermal regions for local sweat stimulation. As illustrated in Figure 3a, this process stimulates sweat glands. Once iontophoresis is finished, the hydrogel is removed and sweating can be observed on the subject's wrist. A commercially available Macroduct® sweat collector is then sealed on the subject's wrist to accumulate sweat for half an hour. Hence, sweat is collected from 35 minutes to 65 minutes after drug intake.

The collected sweat samples are analyzed with DPV measurement to determine the caffeine contents of sweat. Figure 3b and Figure S2 (Supporting Information) show that as caffeine intake increases, the collected sweat samples also contain higher caffeine levels. The functional correlation between DPV-measured caffeine concentration in sweat and caffeine intake is plotted in Figure 3c. The correlation between sweat caffeine concentration and caffeine intake is highly linear with Pearson's correlation coefficient of 0.98, and the slope demonstrates a sensitivity of 45 μM/g. This observation is consistent with the literature,[41,46,47] indicating that the *s*-band can accurately inform users about their caffeine intake.

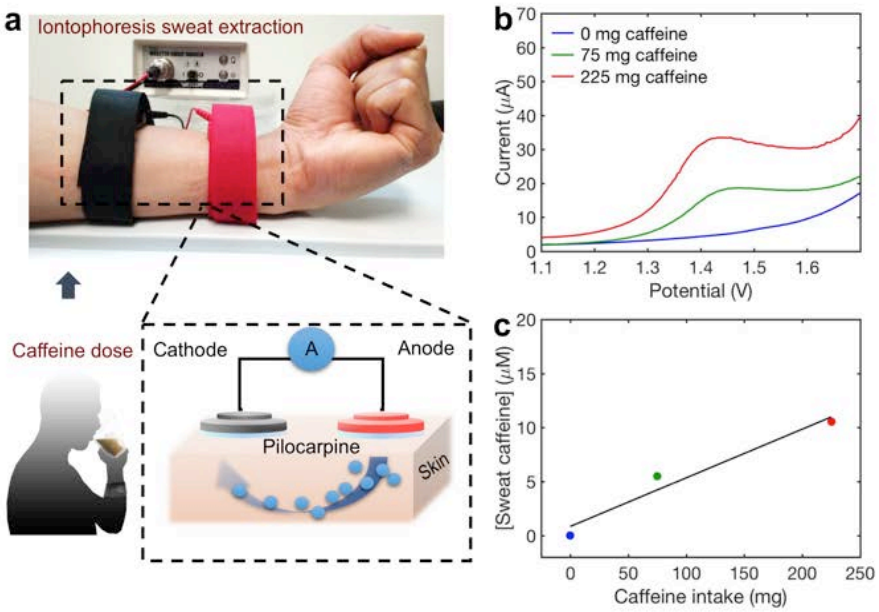

Figure 3. Caffeine monitoring through iontophoresis induced sweat. a) Schematic of iontophoresis-based sweat extraction. The subject consumes 0 mg, 75 mg and 225 mg caffeine, respectively. An iontophoresis current of 1 mA is applied on a subject's wrist for 5 minutes. b) Sensor response in human sweat samples for all caffeine intake conditions. c) The corresponding sweat caffeine concentration observed upon different caffeine intake. (Reprinted with permission from John Wiley and Sons).

In order to demonstrate the sensor's ability to capture physiological trends of caffeine in human subjects, two types of ergometer-based cycling experiments were conducted. Figure 4a shows a time progression panel, indicating time of caffeine intake and exercise period of the first experiment. The subject engages in a constant-load 100 W cycling at 30 minutes after consuming a single-shot espresso coffee (~75 mg caffeine). In most cases, sweat secretion and collection begin approximately 10 minutes after the start of the exercise. Perspiration continues throughout the exercise trial, and sweat caffeine concentration is evaluated at different points in time using the collected sweat samples. Figure 4a shows that the caffeine concentration initially increases, reaches its peak value of 13 µM around 60 min after caffeine intake, and subsequently decreases. The time corresponding to the maximum concentration falls within the expected range of 30 – 120 minutes.[48] Figure 4b-e shows the representative time-stamped plots of the pulse voltammetry results corresponding to Figure 4a.

The observed caffeine concentration trend is consistent with previously reported *ex-situ* data.[46-49] The initial increase in caffeine levels is due to absorption

of caffeine into the human circulatory system, and the subsequent decline is due to catabolism of caffeine.[47-49] In regular healthy subjects, caffeine physiological levels reach their peak values approximately within two hours, and then the caffeine concentrations are projected to diminish.[48] Hence, in Figure 4f, a second experiment is designed with the same subject cycling under identical conditions, with the exception that the cycling time starts at 120 minutes after caffeine intake. In this trial, the caffeine levels begin with a value of 7 μM and show a decreasing trend almost monotonically, which is consistent with our expectation. The concentrations of caffeine in sweat are also lower (2-7 μM) than those in the previous trial after reaching the peak (12-13 μM in Figure 4d,e). These evidences indicate that the caffeine sensor can capture the metabolic behaviors of caffeine. Likewise, Figure 4g-j shows the corresponding time-stamped plots. This set of experiments demonstrates that the caffeine sensor can inform users about the dynamic pharmacokinetics of caffeine.

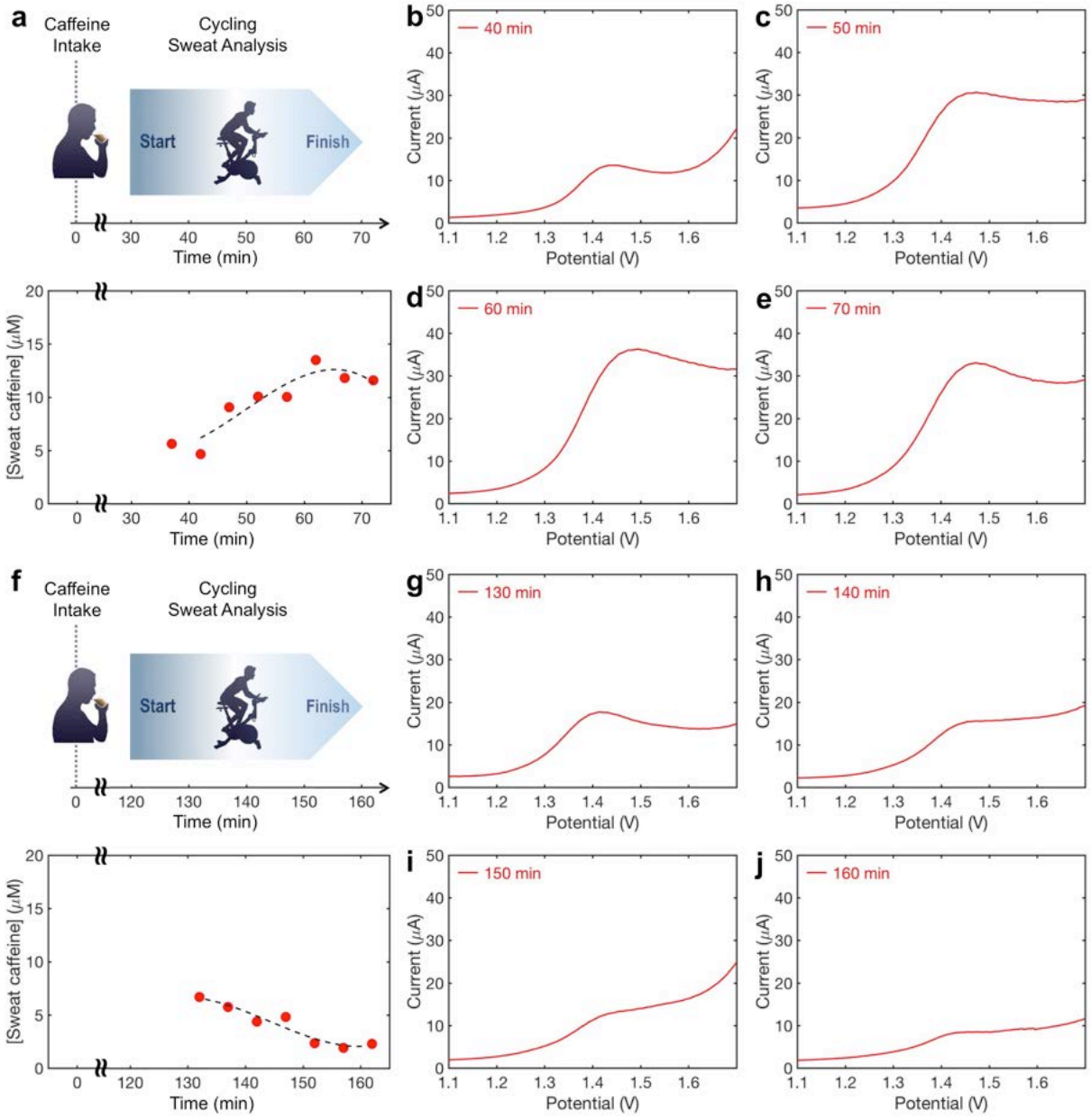

Figure 4. Caffeine monitoring through exercise induced sweat. a) Panel indicating the timeline of the first exercise trial and a summary plot of the caffeine levels over time. The exercise begins at 30 minutes after caffeine intake. b-e) Representative time-stamped plots of the sensor response corresponding to the first experiment. f) Panel indicating the timeline of the second exercise trial and a summary plot of the caffeine levels over time. The exercise begins at 120 minutes after caffeine intake. g-j) Representative time-stamped plots of the sensor response corresponding to the second experiment. (Reprinted with permission from John Wiley and Sons).

2.5 On-body Sweat Analysis

An application of the caffeine sensor is shown in Figure 5a,b with a fully packaged wearable platform. The roll-to-roll printed electrodes connected with the PCB is comfortably worn on a subject's wrist and sealed with a polydimethylsiloxane (PDMS) band. The PCB is assembled using a microcontroller and programmed with a DPV sensing module and can be activated at different time points during the exercise to evaluate sweat caffeine levels. The current peaks in DPV plots are converted to sweat caffeine concentrations using Figure 5c, which is extracted from Figure S3 (Supporting Information). The signal to noise ratio in sweat solution, computed as the current peak (40 μM curve) divided by half of the fluctuation in the baseline reading without caffeine (0 μM curve, 1.1 to 1.2 V) in Figure S3 (Supporting Information), is found to be 14.

The subject performs an exercise trial in which cycling begins at 30 minutes after consuming a single-shot espresso coffee (~75 mg caffeine). The result is summarized in Figure 5d with current peaks extracted from Figure S4 (Supporting Information). In Figure 5d, the detection in sweat solution is limited by the current peak response variations between the roll-to-roll printed electrodes (Experiental Section). Upon conversion with Figure 5c, this corresponds to a detection limit of 3 μM. In addition, we observed that sweat caffeine concentration before caffeine ingestion was consistently below the detection limit. In contrast, the sweat caffeine concentration after caffeine ingestion could be up to 11 μM. The sweat caffeine concentration increases until its peak value of 11 μM at 60 min after caffeine intake, and the concentration subsequently decreases. The data in this on-body experiment follows a similar pattern to the *ex-situ* data in Figure 4, and it demonstrates that the *s*-band technology can potentially be applied in clinical or other practical settings to offer users valuable information regarding their drug intake and metabolism.

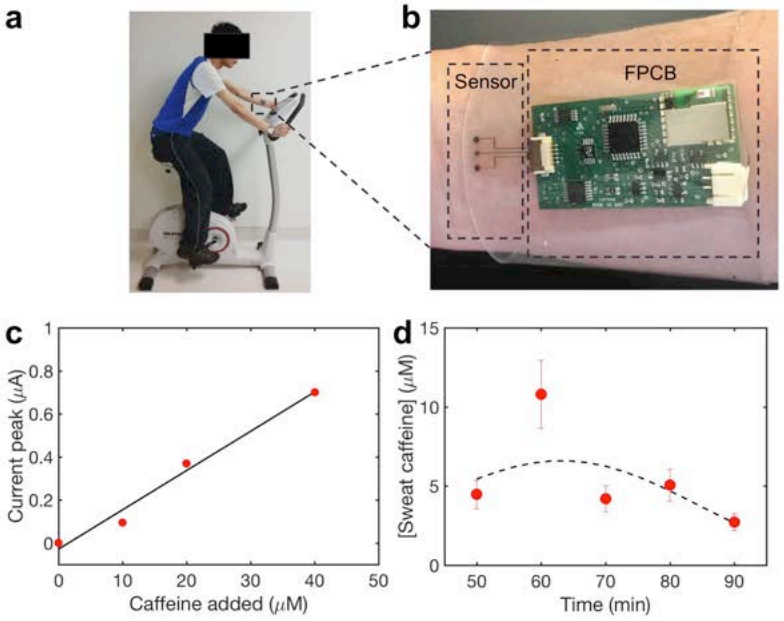

Figure 5. *In-situ* monitoring of caffeine levels using the *s*-band. a) Image of a subject in a cycling exercise and b) a zoom-in image of the *s*-band drug sensing platform packaged in a PDMS wristband. c) Calibration curve for the *s*-band platform in sweat samples. d) Measured sweat caffeine levels during the cycling experiment. The horizontal axis indicates the time elapsed after the subject consumes a single-shot espresso (~75 mg caffeine); the subject begins cycling at 30 min after caffeine intake. (Reprinted with permission from John Wiley and Sons).

2.6 References

(1) Pirmohamed, M. Adverse Drug Reactions as Cause of Admission to Hospital: Prospective Analysis of 18 820 Patients. *British Med. J.* **2004**, *329*, 15-19.

(2) Steiner, R. R.; Larson, R. L. Validation of the Direct Analysis in Real Time Source for Use in Forensic Drug Screening. *J. Forensic Sci.* **2009**, *54*, 617-622.

(3) Wells, K., Klap, R., Koike, A.; Sherbourne, C. Ethnic Disparities in Unmet Need for Alcoholism, Drug Abuse, and Mental Health Care. *Am. J. Psychiatry* **2001**, *158*, 2027-2032.

(4) Hofman, L. F. Human Saliva as a Diagnostic Specimen. *J. Nutrition*. **2001**, *131*, 1621-1625.

(5) Friedrich, J., Seidel, C., Ebner, R.; Kunz-Schughart, L. A. Spheroid-based Drug Screen: Considerations and Practical Approach. *Nat. Protocols* **2009**, *4*, 309-324.

(6) Cone, E. J., Caplan, Y. H., Black, D. L., Robert, T.; Moser, F. Urine Drug Testing of Chronic Pain Patients: Licit and Illicit Drug Patterns. *J. Anal. Toxicology* **2008**, *32*, 530-543.

(7) Rivory, L. P., Slaviero, K. A., Hoskins, J. M.; Clarke, S. J. The Erythromycin Breath Test for the Prediction of Drug Clearance. *Clin. Pharmacokinetics* **2001**, *40*, 151-158.

(8) Kronstrand, R. Nyström, I., Strandberg, J.; Druid, H. Screening for Drugs of Abuse in Hair with Ion Spray LC–MS–MS. *Forensic Sci. Int.* **2004**, *145*, 183-190.

(9) Huestis, M. A., Cone, E. J., Wong, C. J., Umbricht, A.; Preston, K. L. Monitoring Opiate Use in Substance Abuse Treatment Patients with Sweat and Urine Drug Testing. *J. Anal. Toxicology* **2000**, *24*, 509-521.

(10) Johnson, H. L.; Maibach, H. I. Drug Excretion in Human Eccrine Sweat. *J. Investiative. Derm.* **1971**, *56*, 182-188.

(11) Morris, D.; Coyle, S.; Wu, Y.; Lau, K. T.; Wallace, G.; Diamond, D. Bio-sensing Textile Based Patch with Integrated Optical Detection System for Sweat Monitoring. *Sens. Actuators B Chem.* **2009**, *139*, 231-236.

(12) Kintz, P., Tracqui, A., Mangin, P.; Edel, Y. Sweat Testing in Opioid Users with a Sweat Patch. *J. Anal. Toxicology* **1996**, *20*, 393-397.

(13) Lee, J.; Pyo, M.; Lee, S.-H.; Kim, J.; Ra, M.; Kim, W.-Y.; Park, B. J.; Lee, C. W.; Kim, J.-M. Hydrochromic Conjugated Polymers for Human Sweat Pore Mapping. *Nat. Commun.* **2014**, *5*, 3736.

(14) Gao, W.; Emaminejad, S.; Nyein, H. Y. Y.; Challa, S.; Chen, K.; Peck, A.; Fahad, H. M.; Ota, H.; Shiraki, H.; Kiriya, D.; Lien, D.-H.; Brooks, G. A.; Davis, R. W.; Javey, A. Fully Integrated Wearable Sensor Arrays for Multiplexed *in Situ* Perspiration Analysis. *Nature* **2016**, *529*, 509−514.

(15) Wang, C.; Hwang, D.; Yu, Z.; Takei, K.; Park, J.; Chen, T.; Ma, Bi.; Javey, A. User-interactive Electronic-skin for Instantaneous Pressure Visualization. *Nat. Mater.* **2013**, *12*, 899-904.

(16) Takei, K.; Takahashi, T.; Ho, J. C.; Ko, H.; Gillies, A. G.; Leu, P. W.; Fearing, R. S.; Javey, A. Nanowire Active Matrix Circuitry for Low-voltage Macro-scale Artificial Skin. *Nat. Mater*. **2010**, *9*, 821–826.

(17) Ota, H.; Chen, K.; Lin, Y.; Kiriya, D.; Shiraki, H.; Yu, Z.; Ha, T.-J.; Javey, A. Highly-deformable Liquid-state Heterojunction Sensors. *Nat. Commun* **2014**, *5*, 5032.

(18) Ota, H.; Chao, M.; Gao, Y.; Wu, E.; Tai, L.-C.; Chen, K.; Matsuoka, Y.; Iwai, K.; Fahad, H. M.; Gao, W.; Nyein, H. Y. Y.; Lin, L., Javey, A. 3D Printed Earable Smart Devices for Real-time Detection of Core Body Temperature. *ACS Sens*. **2017**, *2*, 990-997.

(19) Emaminejad, S.; Gao, W.; Wu, E.; Davies, Z. A.; Yin Yin Nyein, H.; Challa, S.; Ryan, S. P.; Fahad, H. M.; Chen, K.; Shahpar, Z.; Talebi, S.; Milla, C.; Javey, A.; Davis, R. W. Autonomous Sweat Extraction and Analysis Applied to Cystic Fibrosis and Glucose Monitoring Using a Fully Integrated Wearable Platform. *Proc. Natl. Acad. Sci. U. S. A.* **2017**, *114*, 4625−4630.

(20) Gao, W.; Nyein, H. Y. Y.; Shahpar, Z.; Fahad, H. M.; Chen, K.; Emaminejad, S.; Gao, Y.; Tai, L.-C.; Ota, H.; Wu, E.; Bullock, J.; Zeng, Y.; Lien, D.-H.; Javey, A. Wearable Microsensor Array for Multiplexed Heavy Metal Monitoring of Body Fluids. *ACS Sens.* **2016**, *1*, 866–874.

(21) Nyein, H. Y. Y.; Gao, W.; Shahpar, Z.; Emaminejad, S.; Challa, S.; Chen, K.; Fahad, H. M.; Tai, L.-C.; Ota, H.; Davis, R. W.; Javey, A. A Wearable Electrochemical Platform for Non-invasive Simultaneous Monitoring of Ca^{2+} and pH. *ACS Nano* **2016**, *10*, 7216–7224.

(22) Imani, S.; Bandodkar, A. J.; Mohan, A. M. V.; Kumar, R.; Yu, S.; Wang, J.; Mercier, P. P. A Wearable Chemical–electrophysiological Hybrid Biosensing System for Real-time Health and Fitness Monitoring. *Nat. Commun* **2016**, *7*, 11650.

(23) Kim. J.; Jeerapan, I.; Imani, S.; Cho, T. N.; Bandodkar, A.; Cinti, S.; Mercier, P. P.; Wang, J. Non-invasive Alcohol Monitoring Using a Wearable Tattoo-based Iontophoretic-biosensing System. *ACS Sens.* **2016**, *1*, 1011–1019.

(24) Koh. A.; Kang, D.; Xue, Y.; Lee, S.; Pielak, R. M.; Kim, J.; Hwang, T.; Min, S.; Banks, A.; Bastien, P.; Manco, M. C.; Wang, L.; Ammann, K. R.; Jang, K.-I.; Won, P.; Han, S.; Ghaffari, R.; Paik, U.; Slepian, M. J.; Balooch, G.; Huang, Y.; Rogers, J. A. A Soft, Wearable Microfluidic Device for the Capture, Storage, and Colorimetric Sensing of Sweat. *Sci. Transl. Med.* **2016**, *8*, 366ra165.

(25) Lee, H.; Choi, T. K.; Lee, Y. B.; Cho, H. R.; Ghaffari, R.; Wang, L.; Choi, H. J.; Chung, T. D.; Lu, N.; Hyeon, T.; Choi, S. H.; Kim, D.-H. A Graphene-based Electrochemical Device with Thermoresponsive Microneedles for Diabetes Monitoring and Therapy. *Nature Nanotechnol.* **2016**, *11*, 566-572.

(26) Bandodkar, A. J.; Molinnus, D.; Mirza, O.; Guinovart, T.; Windmiller, J. R.; Valdés-Ramírez, G.; Andrade, F. J.; Schöning, M. J.; Wang, J. Epidermal Tattoo Potentiometric Sodium Sensors with Wireless Signal Transduction for Continuous Non-invasive Sweat Monitoring. *Biosens. Bioelectron.* **2014**, *54*, 603-609.

(27) Jia, W.; Bandodkar, A. J.; Valdés-Ramírez, G.; Windmiller, J. R.; Yang, Z.; Ramírez, J.; Chan, G.; Wang, J. Electrochemical Tattoo Biosensors for Real-time Noninvasive Lactate Monitoring in Human Perspiration. *Anal. Chem*. **2013**, *85*, 6553–6560.

(28) Xu, S.; Zhang, Y.; Jia, L.; Mathewson, K. E.; Jang, K.-I.; Kim, J.; Fu, H.; Huang, X.; Chava, P.; Wang, R.; Bhole, S.; Wang, L.; Na, Y. J.; Guan, Y.; Flavin, M.; Han, Z.; Huang, Y.; Rogers, J. A. Soft Microfluidic Assemblies of Sensors, Circuits, and Radios for the Skin. *Science* **2014**, *344*, 70–74.

(29) Lipomi, D. J.; Vosgueritchian, M.; Tee, B. C.-K.; Hellstrom, S. L.; Lee, J. A.; Fox, C. H.; Bao, Z. Skin-like Pressure and Strain Sensors Based on Transparent Elastic Films of Carbon Nanotubes. *Nature Nanotechnol*. **2011**, *6*, 788–792.

(30) McAlpine, M. C., Ahmad, H., Wang, D.; Heath, J. R. Highly Ordered Nanowire Arrays on Plastic Substrates for Ultrasensitive Flexible Chemical Sensors. *Nature Mater*. **2007**, *6*, 379–384.

(31) Kaltenbrunner, M.; Sekitani, T.; Reeder, J.; Yukota, T.; Kuribara, K.; Tokuhara, T.; Drack, M.; Schwödiauer, R.; Graz, I.; Bauer-Gogonea, S.; Bauer, S.; Someya, T. An Ultra-lightweight Design for Imperceptible Plastic Electronics. *Nature* **2013**, *499*, 458–463.

(32) Kim, D. H.; Lu, N.; Ma, R.; Kim, Y. S.; Kim, R. H.; Wang, S.; Wu, J. Won, S. M.; Tao, H.; Islam, A.; Yu, K. J.; Kim, T. I.; Chowdhury, R.; Ying, M.; Xu, L.; Li, M.; Chung, H. J.; Keum, H.; McCormick, M.; Liu, P.; Zhang, Y. W.; Omenetto, F. G.; Huang, Y.; Coleman, T.; Rogers, J. A. Epidermal Electronics. *Science* **2011**, *333*, 838–843.

(33) Dogan-Topal, B., Uslu, B.; Ozkan, S. A. Voltammetric studies on the HIV-1 inhibitory drug Efavirenz: The Interaction between dsDNA and Drug Using Electrochemical DNA Biosensor and Adsorptive Stripping Voltammetric Determination on Disposable Pencil Graphite Electrode. *Biosens. Bioelectron.* **2009**, *24*, 2358-2364.

(34) Erdem, A., Karadeniz, H.; Caliskan, A. Dendrimer Modified Graphite Sensors for Detection of Anticancer Drug Daunorubicin by Voltammetry and Electrochemical Impedance Spectroscopy. *Analyst* **2011**, *136*, 1041-1045.

(35) Erderm, A.; Ozsoz, M. Interaction of the Anticancer Drug Epirubicin with DNA. *Anal. Chim. Acta* **2001**, *437*, 107-114.

(36) Zhao, F.; Wang, F.; Zhao, W.; Zhou, J.; Liu, Y.; Zou, L.; Ye, B. Voltammetric Sensor for Caffeine Based on a Glassy Carbon Electrode Modified with Nafion and Graphene Oxide. *Microchim. Acta* **2011**, *174*, 383-390.

(37) Hartley, T. R., Lovallo, W. R.; Whitsett, L. Cardiovascular Effects of Caffeine in Men and Women. *Am. J. Cardiol*. **2004**, *93*, 1022-1026.

(38) Noordzij, M.; Uiterwaal, C. S. P. M.; Arends, L. R.; Kok, F. J.; Grobbee, D. E.; Geleijnse, J. M. Blood Pressure Response to Chronic Intake of Coffee and Caffeine: a Meta-analysis of Randomized Controlled Trials. *J. Hypertens*. **2005**, *23*, 921-928.

(39) Ruusunen, A.; Lehto, S. M.; Tolmunen, T.; Mursu, J.; Kaplan, G. A.; Voutilainen, S. Coffee, Tea and Caffeine Intake and the Risk of Severe Depression in Middle-aged Finnish Men: the Kuopio Ischaemic Heart Disease Risk Factor Study. *Public Health Nutr*. **2010**, *13*, 1215-1220.

(40) Spriet, L. L. Caffeine and Performance. *Int. J. Sport Nutr*. **1995**, *5*, 84-99.

(41) Kovacs E. M. R., Stegen, J. C. H.; Brouns, F. Effect of Caffeinated Drinks on Substrate Metabolism, Caffeine Excretion, and Performance. *J. Appl. Physiol.* **1998**, *85*, 709–715.

(42) Birkett, D. J.; Miners, J. O. Caffeine renal clearance and urine caffeine concentrations during steady state dosing. Implications for Monitoring Caffeine Intake during Sports Events. *Br. J. Clin. Pharmacol*. **1991**, *31*, 405-408.

(43) Lee, W.; Koo, H.; Sun, J.; Noh, J.; Kwon, K.-S.; Yeom, C.; Choi, Y.; Chen, K.; Javey, A.; Cho, G. A Fully Roll-to-roll Gravure-printed Carbon Nanotube-based Active Matrix for Multi-touch Sensors. *Sci. Rep*. **2015**, *5*, 17707.

(44) Keefer, E. W., Botterman, B. R., Romero, M. I., Rossi, A. F.; Gross, G. W. Carbon Nanotube Coating Improves Neuronal Recordings. *Nature Nanotechnol*. **2008**, *3*, 434–439.

(45) McCusker, R. R., Goldberger, B. A.; Cone, E. J. Caffeine Content of Specialty Coffees. *J. Anal. Toxicol*. **2003**, *27*, 520-522.

(46) Graham, T. E.; Spriet, L. L. Metabolic, Catecholamine, and Exercise Performance Responses to Various Doses of Caffeine. *J. Appl. Physiol.* **1995**, *78*, 867–874.

(47) Bell, D. G.; McLellan T. M. Exercise Endurance 1, 3, and 6 h after Caffeine Ingestion in Caffeine Users and Nonusers. *J. Appl. Physiol.* **2002**, *93*, 1227–1234.

(48) Collomp, K. Effects of Moderate Exercise on the Pharmacokinetics of Caffeine. *Eur J Clin Pharmacol.* **1991**, *40*, 279-282.

(49) Tsuda T., Noda, S., Kitagawa, S.; Morishita, T. Proposal of Sampling Process for Collecting Human Sweat and Determination of Caffeine Concentration in It by Using GC/MS. *Biomed Chromatogr.* **2000**, *14*, 505-510.

2.7 Appendix

Sensor Array Fabrication and Preparation. The electrode arrays were fabricated on top of flexible PET film via roll-to-roll printing technique at Sunchon National University. Specifically, the electrodes were fabricated with roll-to-roll gravure printing on polyethylene terephthalate substrate (SKC Korea AH71D). The silver (Ag), carbon (C) and insulation layers were printed in sequence. Ag ink was acquired (Paru Solar Energy Company PG-007) and reformulated by dispersing Ag in solution (InkTec TEC-PR-041) to enhance the Ag ink's stability. For the Ag ink, the surface tension and viscosity were improved by addition of 10 % polyvinyl butyral in Terpineol (Sigma Aldrich). During the printing, temperature and humidity were controlled to be 23 ± 2 °C and 35 ± 2 %, respectively, to maintain the accuracy of printing to be ± 20 μm. Post-printing drying of the Ag electrodes was performed by passing the electrodes through a 150 °C chamber for 5 seconds at 6 m / min. The working electrode and reference electrode were further processed. Carbon paste (Dozen TECH Korea DC-15) was diluted by adding diethylene glycol monoethyl ether acetate (ECA) until 350 cp viscosity was reached. Afterwards, the carbon paste was printed to cover the Ag layer. The drying process was performed in 150 °C chamber for 5 seconds. Finally, the insulating ink was prepared by dissolving polyethylene resin (Daejung Chemicals and Metals. 20 g) in ECA (80 mL) to passivate the Ag layers. The printing speed of the insulating layer was 6 m / min.

The electrodes were annealed at 150 °C for 1 hour (MTI Corporation Vacuum Oven). The working and counter electrodes were cleaned in a 8 M HNO_3 solution for 10 seconds to remove the exposed Ag. 0.1 M $FeCl_3$ solution (0.80 μL) was injected on top of the Ag reference electrode for 10 seconds to produce a uniform Ag/AgCl film. 0.01% multiwall carbon nanotubes (MWCNT, 0.84 μL) and 0.01% Nafion 117 (Sigma Aldrich, 0.84 μL) were subsequently drop-casted onto the working electrode and annealed at room temperature till dry for 15 hours.

Characterization of the Sensor. The printed electrodes were characterized electrochemically by performing DPV measurements in 0-40 μM caffeine solutions (dissolved in 0.01 M acetate buffer solution (pH 4.6)). CHI 1230C potentiostat (CH Instruments) was used for DPV measurements (initial potential: 1.1 V; final potential: 1.7 V; increment: 4 mV; amplitude: 50 mV; pulse width: 50 ms; sample width: 15 ms; pulse period: 100 ms). The modified working electrode was used here with commercially available Ag/AgCl reference electrode and platinum wire counter electrode. The sensor's selectivity was evaluated by addition of selected analytes (urea, glucose, lactate, ascorbic acid, pilocarpine) to 40 μM of caffeine in the acetate buffer solutions. The concentrations of the analytes were decided according to their physiologically relevant concentrations. Baselines in the

I-V plots of the DPV measurements were normalized such that they were aligned. DPV measurements of 40 μM caffeine were performed once for all of the roll-to-roll printed working electrodes to eliminate the ones with outlying performances (selected the ones with peak current variations within 20%, which defines the error in the experiments).

Ex-situ Iontophoresis Sweat Analysis. Iontophoresis sweat extraction was performed by firstly placing pilocarpine hydrogel (ELITechGroup SS-023 Pilogel® Discs) underneath the anode and cathode electrodes followed by applying a 1-mA DC current for 5 minutes to drive the pilocarpine into the sub-dermal regions of a subject to stimulate sweat glands (ELITechGroup Model 3700 Webster Sweat Inducer). Afterwards, a commercial Macroduct® collector was tightly sealed around the subject's wrist to allow sweat collection for 30 minutes. The collected sweat samples were analyzed with CHI 1230C potentiostat (CH Instruments) using DPV measurements. To improve the sensitivity, accumulation of caffeine molecules at -1.2 V for 30 seconds was applied prior to DPV analysis. The current peaks measured with DPV were converted to sweat concentrations via calibrations, which were obtained via addition of caffeine to sweat samples similar to that in Figure S3 (Supporting Information). Other conditions, the same as those in the characterization experiments.

Ex-situ Exercise Sweat Analysis. The subjects performed cycling exercise on a stationary ergometer (Kettler E3 Upright Exercise Bike) with 100 W power output. Once the subjects started sweating, sweat samples were collected every 5 minutes using centrifuge tubes from the foreheads of the subjects. After each collection, the subjects cleaned their foreheads with gauze. The evaluation of sweat samples followed the same procedure as that in the *ex-situ* iontophoresis sweat analysis.

In-situ Exercise Sweat Analysis. The on-body analysis of the *s*-band was approved by the institutional review board at the University of California, Berkeley (CPHS 2016-06-8853). The *s*-band was packaged with a polydimethylsiloxane (PDMS) transparent band on top of the sensor and around the subject's wrist, as shown in Figure 5b. At different time throughout the exercise trial, the *s*-band was activated to perform the *in situ* DPV measurements. The raw data was then transmitted via Bluetooth wirelessly to a user interface (CoolTerm serial-port terminal application), normalized to a common baseline current, and filtered (MATLAB® Hampel and Smooth functions) for caffeine level monitoring on a computer. Curve fitting was performed and plotted as the dotted line (MATLAB® Weibull function). A schematic diagram of the *s*-band's circuit design is shown in Figure S5 (Supporting Information).

Signal Conditioning, Processing and Wireless Transmission Circuit Design. The circuit diagram of the analog signal-conditioning block of the device

is shown in Figure S5 (Supporting Information). The entire circuit mimics the DPV measurements of the potentiostat instrument. At the core of our system we use an Atmega328p (Atmel 8-bit) (Microchip Technology) microcontroller that can be programmed on-board by a pocket AVR programmer from Sparkfun. The microcontroller communicates with a 16-bit digital-to-analog converter (DAC) DAC8552 (Texas Instrument) through SPI (Serial Peripheral Interface) protocol. The DAC sets two voltages: one for working electrode and the other one for reference electrode. The DPV parameters follow the same as those in the potentiostat's settings, including initial potential, final potential, increment, amplitude, pulse width, sample width and pulse period. The voltage for reference electrode is low-pass filtered by the fourth order Sallen-Key topology to provide stable reference. The current from the working electrode is converted into voltage by low-pass transimpedance amplifiers. The voltage is then measured by a 16-bit analog-to-digital converter (ADC) LTC1864 (Linear Technology). The ADC sends the voltage data to the microcontroller through SPI protocol. The microcontroller transmits the data to the Bluetooth transceiver using the Universal Asynchronous Receiver/Transmitter (UART) protocol. The Bluetooth then communicates with the mobile phone or computer.

Power Delivery to the DPV Board. The PCB is powered by a single rechargeable lithium ion polymer battery with a nominal voltage of 3.7 V. The equivalent diagram is shown in Figure S5 (Supporting Information). There are 3 paths of power delivery. The first path requires 5.0 V for the digital component of the circuit. This is achieved by using DC-DC converter to boost up the battery voltage from 3.7 V to 5.3 V, and then using low-dropout voltage regulator to obtain a regulated 5.0 V voltage. The second path uses the same strategy, but the voltage is used for the analog portion of the circuit. The third path uses only the low-dropout voltage regulator to realize a regulated 3.3 V potential for the Bluetooth module.

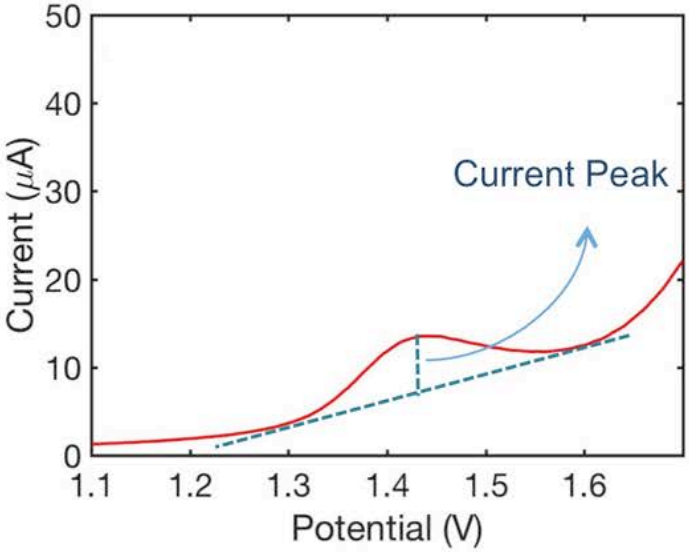

Figure S1. Measurement of the peak height from a DPV measurement. The peak height is the length of the vertical line connecting the peak position and the tangent line to the DPV curve. (Reprinted with permission from John Wiley and Sons).

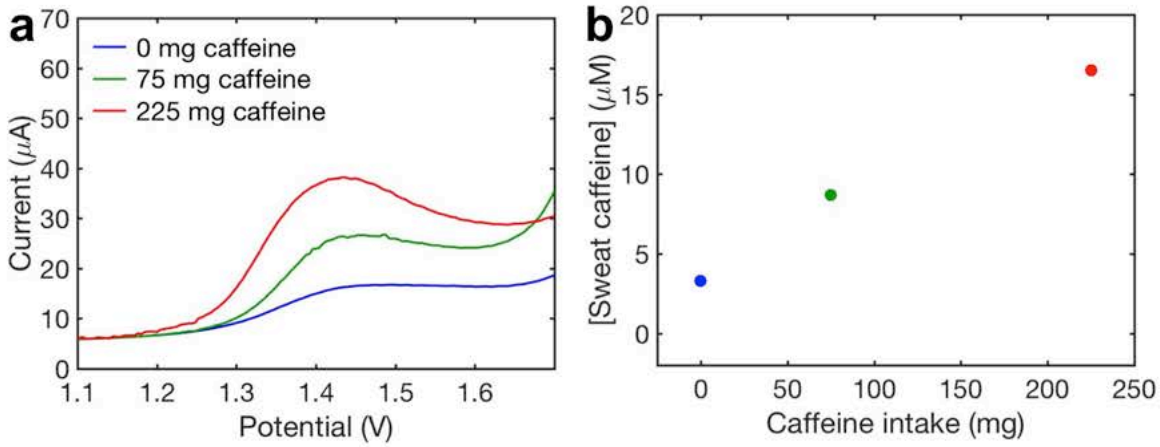

Figure S2. Caffeine monitoring through iontophoresis induced sweat samples (subject II). a) Sensor response in the sweat samples for all caffeine intake conditions and b) the corresponding sweat caffeine concentration observed upon different caffeine intake. (Reprinted with permission from John Wiley and Sons).

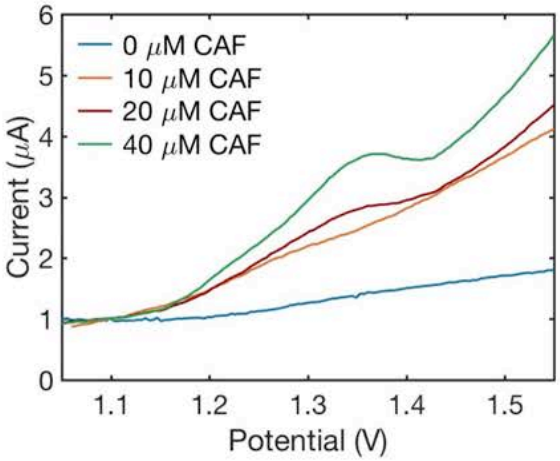

Figure S3. Calibration for the *s*-band platform in sweat samples. Results of the DPV measurements in sweat samples collected from the same subject in Figure 5. (Reprinted with permission from John Wiley and Sons).

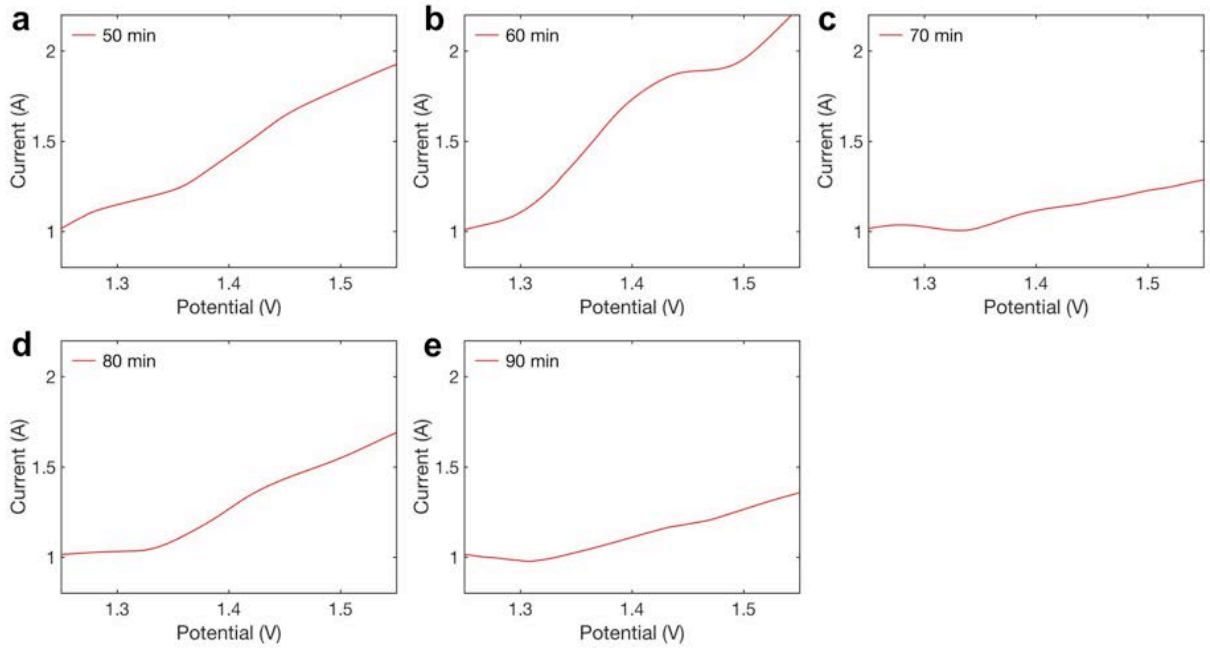

Figure S4. *In-situ* caffeine monitoring through exercise induced sweat. a-e) Representative time-stamped plots of sensor response corresponding to the *in-situ* experiment in Figure 5. (Reprinted with permission from John Wiley and Sons).

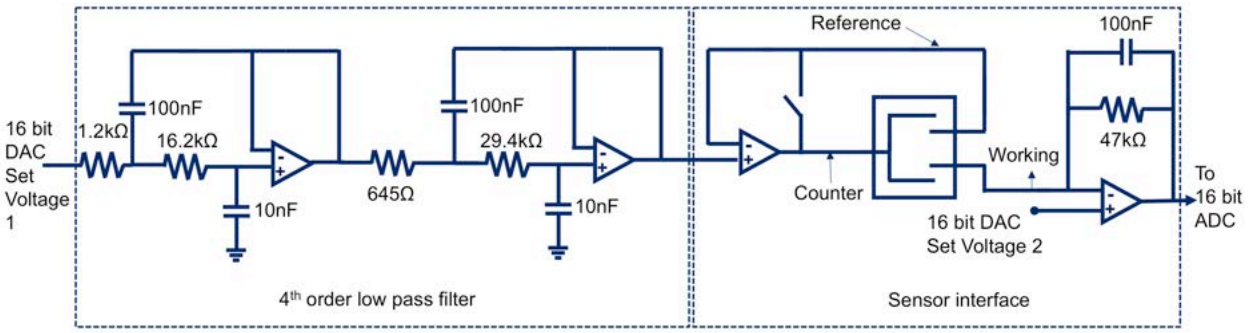

Figure S5. Schematic of the *s*-band platform's voltammetry circuit. The circuit incorporates three terminals, which correspond to the working, reference and counter electrodes. (Reprinted with permission from John Wiley and Sons).

Chapter 3 Levodopa Monitoring with Wearable Sweat Sensors

The following chapter has been previously published in a similar format.

Reprinted (adapted) with permission from (Tai, L.-C.; Liaw, T. S.; Lin, Y.; Nyein, H. Y. Y.; Bariya, M.; Ji, W.; Hettick, M.; Zhao, C.; Zhao, J.; Hou, L.; Yuan, Z.; Fan, Z.; Javey, A. Wearable Sweat Band for Noninvasive Levodopa Monitoring. *Nano Lett.* **2019**, *19*, 6346-6351).

3.1 Introduction to Levodopa and Parkinson's Disease

Levodopa is the medication administered to treat patients with Parkinson's disease.[1-7] Despite its success, an individual's responses to levodopa can vary due to factors such as dietary intake, age, gender and drug administration history.[8-12] These variations can lead to unfavorable fluctuations of the subject's motor and cognitive functions if the levodopa dosage is not tailored towards the individuals.[12-14] Therefore, levodopa monitoring is an essential part of the treatment for Parkinson's disease. The gold standard for optimizing levodopa dosage involves an assessment of the motor function of a Parkinson's disease patient.[9] This method requires clinicians to evaluate the subject's motor functions, leading to difficulty of point-of-care testing and ambiguity in drug dosage. To address this challenge, monitoring blood levodopa concentration stands out as a viable solution.[15-18] However, blood-based detection is hampered by its need for invasive sampling and separate analytical tools, making it inappropriate for the long-term and frequent measurements that are necessary due to the dynamic nature of drug metabolism.

Taking this into consideration, human sweat is an alternative to blood due to its accessibility through noninvasive procedures and its abundance of biomolecules. Like other drug molecules that undergo xenobiotic metabolism pathway, levodopa excretes through sweat with its concentration in sweat exhibiting a potential correlation with that in human plasma.[19-22] Additionally, under standard levodopa dosage, sweat levodopa level shows up in the micro-molar ranges,[17-19] making it amenable for reliable detection with current technologies.[23,24] For these reasons, sweat presents an ideal means for non-obstructive monitoring of levodopa for dosage optimization. Sweat sensing patches have been employed for drug tests in athletic doping control, drug abuse investigation and forensic inspection.[25,26] Recently, sweat sensors for drugs and their related biomolecules have also been demonstrated via optical and electrochemical techniques.[27-32] In particular, the electrochemical approach represents an attractive method owing to its advantages for electronic integration, economical cost, sensitivity and selectivity.[29-36]

In this work, we expand the strength of the electrochemical sensor through integrated surface innovations at the physical and chemical levels. The incorporation of gold dendritic nanostructures onto the electrodes remarkably enhanced the detection limit of the levodopa sensor down to about 1 μM in sweat solution, a couple times of improvement compared to previous work tested in human fluid.[37] Moreover, the crosslinking mechanisms with glutaraldehyde provides us chemically robust enzymatic structures to achieve sensor stability for long-term and continuous usage.[37-40] This approach effectively connects existing sensor enhancement technologies into a consolidated platform for prolonged sensor operation. Our solutions effectively address the challenges for drug detection, which are attributed to the generally low concentration of drugs in human sweat and the long time scale of drug metabolism.

3.2 Device Background and Sensing Mechanism

The design of the wearable sensor packaged into a sweat band (*s*-band) is illustrated in Figure 1a. The sensor is fabricated on a polyethylene terephthalate (PET) substrate and it employs a standard three-electrode configuration with a functionalized levodopa sensing electrode as working electrode, a Ag/AgCl top layer as reference electrode and a Au top layer as counter electrode. As shown in Figure 1b, during amperometric measurement, levodopa excreted in sweat can be oxidized via tyrosinase enzyme to dopaquinone.[37] This process generates a Faradaic current that can be further calibrated into its corresponding sweat levodopa concentration. The cross-section schematic of the electrodes is shown in Figure 1c, and Figure 1d shows a scanning electron microscope image of the gold dendrite to validate the successful growth and density of the nanostructures. To achieve the enhancement on sensitivity, gold nano-dendrites with largely increased surface area are synthesized via over-potential deposition approach on the evaporated Au/Cr conductive layer.[38,39] Further, thionin acetate salts are deposited via cyclic voltammetry (CV) method conformally on the as-synthesized dendritic gold structure and glutaraldehyde/tyrosinase are drop-casted onto the working electrode. Glutaraldehyde serves as the cross-linker to immobilize the tyrosinase enzyme that facilitates the electrochemical oxidation of levodopa.[37,40] It is also worth mentioning that the dendritic gold plays a pivotal role to provide adequate interface for enzyme loading and molecular contact to achieve an improved sensing performance. The final modification step for the working electrode involves the drop-casting of Nafion, which enhances the long-term stability and anti-fouling features of the electrochemical sensor.[41] The prospective application of the sensor is illustrated in Figure 1e, which shows the application of iontophoresis

for noninvasive and stationary stimulation of sweat to monitor levodopa levels after a subject consumes the drug. The *s*-band enables continuous monitoring of levodopa, which allows for personalized optimization of levodopa dosage.

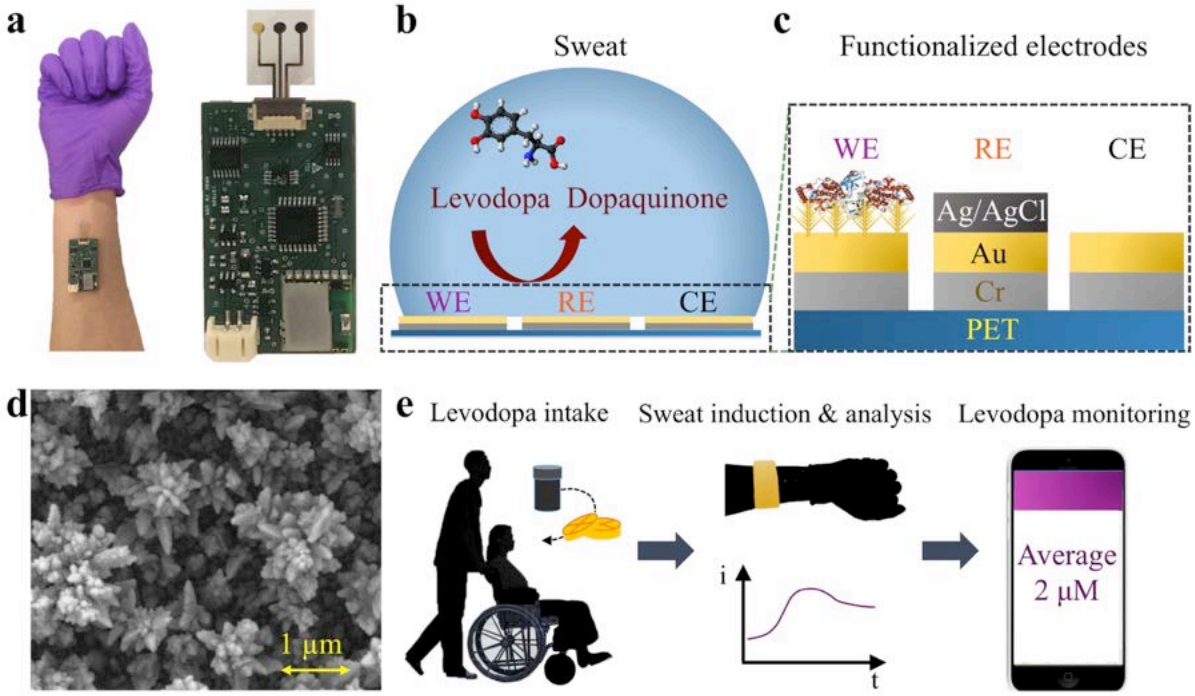

Figure 1. Schematic of the *s*-band and drug sensing mechanism. (a) Optical image of the *s*-band worn on a subject's wrist. (b) Sensing mechanism of the levodopa sensor. WE, RE and CE are working electrode, reference electrode and counter electrode. (c) The cross-section view of the gold electrode on a flexible sensor patch. (d) Scanning electron microscope image of the gold dendritic structure. (e) Real-time sweat levodopa monitoring using the *s*-band after levodopa intake. (Reprinted with permission from American Chemical Society).

3.3 Sensor Characterization

The functionalized levodopa sensing electrode was characterized with CV scanning, which indicates the oxidation peak of levodopa. Figure 2a shows the CV curves using the functionalized electrode in phosphate-buffered saline (PBS) with different concentrations of levodopa. The oxidation and reduction peaks for levodopa are around 0.34 V and 0.30 V (method of peak identification is illustrated in Supporting Information Figure S1), respectively, which are consistent with the literature.[23] Figure 2b shows a CV in the proximity of levodopa's oxidation peak in the physiologically relevant concentration range.[19] The functionalized electrode

responds to levodopa with high sensitivity in the micro-molar range. This is a remarkable enhancement of more than two orders of magnitude compared to the response of a bare Au electrode (Supporting Information Figure S2). Figure 2c shows the amperometric response of levodopa at the oxidation potential (0.34 V). The inset displays the calibration curve with a sensitivity of 15 nA/μM, which is on par with the best levodopa sensors reported.[23] This is notable considering the simplicity of electrode functionalization and the electrode's excellent stability for long-term usage.

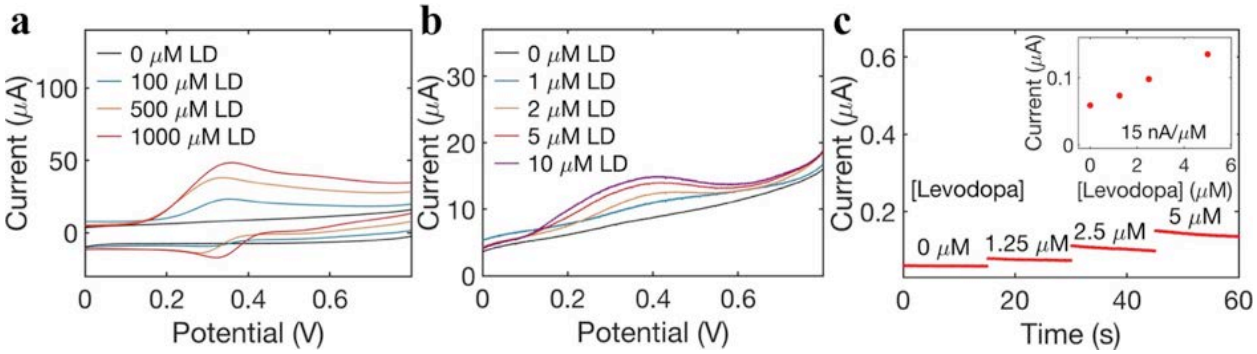

Figure 2. Characterization of the functionalized working electrode in PBS. (a) CV of levodopa (LD) dissolved in PBS and (b) zoom-in view for smaller concentration range. (c) Amperometric response of levodopa dissolved in PBS. Inset shows the calibration curve. (Reprinted with permission from American Chemical Society).

The sensors were further characterized in sweat solution to demonstrate its practical applications for noninvasive monitoring. Figure 3a shows a CV in the proximity of levodopa's oxidation peak, which is identified to be 0.25 V. The amperometric response of levodopa was similarly tested at the oxidation potential, shown in Figure 3b. The corresponding calibration curve in sweat is displayed in Figure 3c, and the sensitivity is found to be 1.7 nA/μM. This value is different from that in PBS and it is expected due to bio-fouling activity.[29] For the purpose of the study, we define drift as the maximum change in the signal of the amperometric response of a fixed concentration (e.g., 10 μM) over a period of operation (e.g., 30 minutes). The sensor drift is approximately 18 nA as shown in Supporting Information Figure S3. The error of concentration measurement due to drift is estimated to be 1.2 μM. The limit of detection is 1.25 μM as shown in Figure 3b. The signal-to-noise ratio (SNR) is the ratio of the square of the amplitude of the signal to the background noise. Based on Supporting Information Figure S3b, the amperometric response signal is found to be 225 nA. During the measurement, the noise level is observed to be approximately 50 nA, which results

in a SNR of 20. The selectivity of the sensor is essential in the presence of other common sweat biomolecules. Therefore, the amperometric response of the addition of levodopa and its potential interferents such as uric acid (20 μM), glucose (166 μM) and ascorbic acid (16 μM) is recorded in Figure 3d. The concentrations are chosen to be in their physiologically relevant ranges.[29-32] The result shows that the interference on the levodopa sensor performance is within an error range of 0.35 μM.

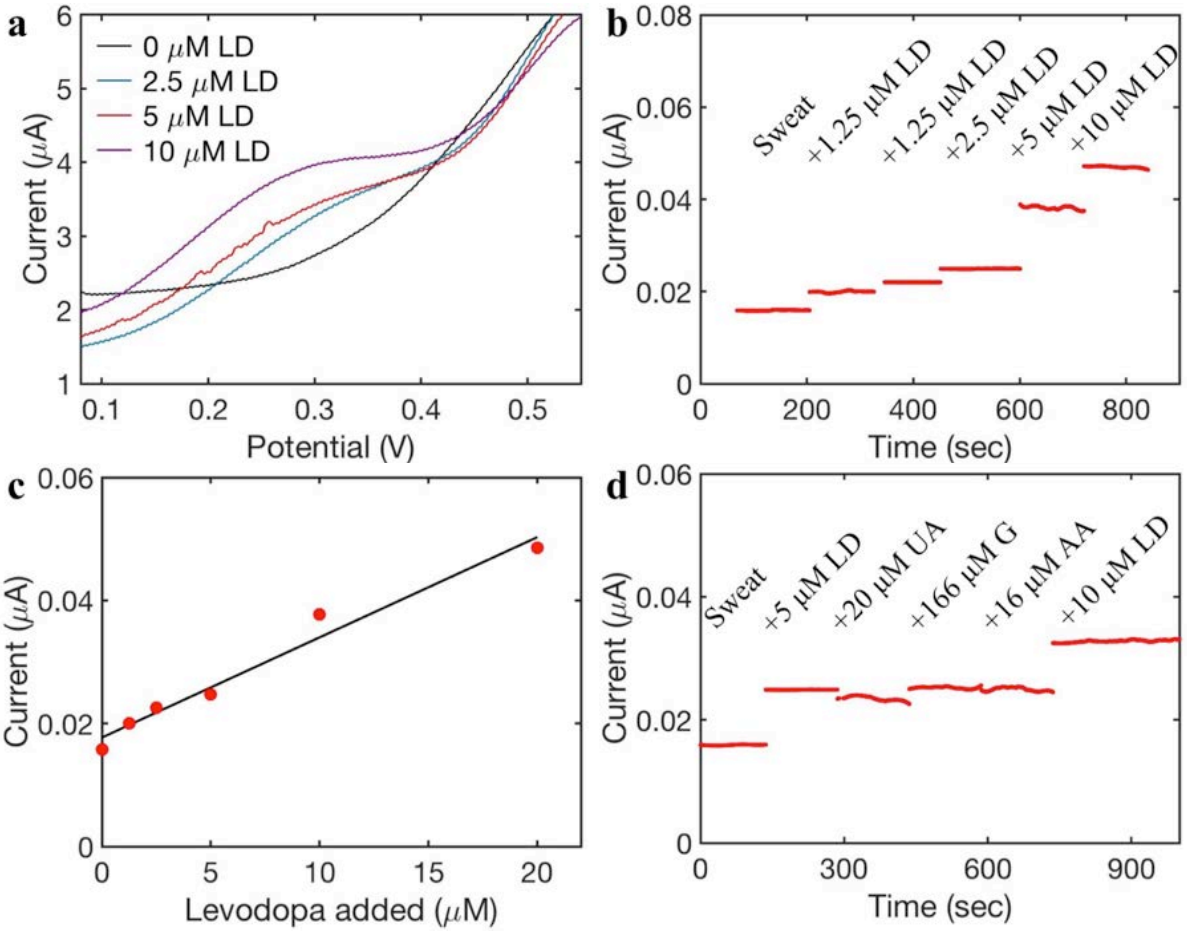

Figure 3. Characterization of the levodopa sensor in sweat solution. (a) CV of levodopa dissolved in sweat. (b) Amperometric response of levodopa dissolved in sweat, and (c) the corresponding calibration curve. (d) Interference study of the levodopa sensor after the addition of levodopa (LD), uric acid (UA), glucose (G) and ascorbic acid (AA). (Reprinted with permission from American Chemical Society).

3.4 Sweat Analysis

To explore the viability of using the *s*-band to track the metabolism of levodopa in human subjects, sweat was extracted from a healthy volunteer through iontophoresis and after *vicia faba* (fava bean) consumption. Fava beans are levodopa-containing legumes consumed for culinary and medicinal purposes.[18] The use of fava beans allows for extensive testing of the *s*-band's functionalities on non-vulnerable, healthy subjects.

Figure 4a shows the time progression panel of fava beans consumption and iontophoresis application, as well as continuous sensor readings of the sweat levodopa concentration. The result demonstrates that the *s*-band can continuously capture the sweat levodopa trend that resembles the blood levodopa profile observed.[15-18] During iontophoretic stimulation, sweating begins after iontophoresis and lasts for about 20 to 45 minutes. Therefore, two consecutive applications of iontophoresis are performed at -20 minutes and 25 minutes, with respect to the time of fava beans intake, to cover a broad time range that captures levodopa's metabolic trend. The subject consumes 450 grams of fava beans after 12 hours of fasting, and its sweat levodopa concentration is monitored after each iontophoresis. The observed sweat levodopa level versus time shows an increasing trend up to 6.6 μM at about 47 minutes, after which the concentration begins to decrease. The levodopa concentration decreases to 3.3 μM at about 74 minutes, so the half-life of the decay is found to be 27 minutes. The time scales of levodopa's half-life and its time of peak concentration are expected based on previous observations.[15-18] In Figure 4b, the subject first consumes a 426-gram sandwich (see Methods), followed by 450 grams of fava beans. Three consecutive applications of iontophoresis are performed at -20, 25 and 80 minutes, with reference to the time of fava beans consumption. The result shows a slight delay of 13 minutes in the pharmacokinetic peak time compared to that in Figure 4a. This finding is expected as dietary intake can affect the pharmacokinetic profile of levodopa in human secretory systems.[11] The data in Figures 4a and 4b verifies the *s*-band's capability of continuous levodopa measurement.

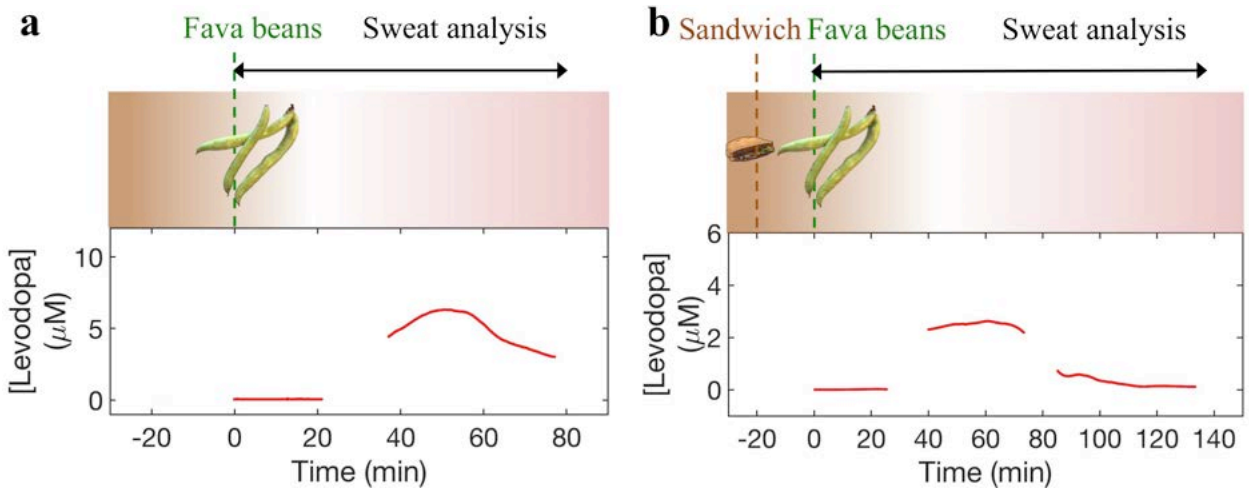

Figure 4. Levodopa monitoring via iontophoresis-induced sweat. Sweat levodopa concentration is monitored continuously after fava beans consumption and subsequent applications of iontophoresis (a) without and (b) with prior dietary consumption. The horizontal axis indicates the time elapsed after the subject consumes 450 mg of fava beans. (Reprinted with permission from American Chemical Society).

While sweating caused by iontophoresis can be limited in its duration, sweating generated through exercise can typically last longer and allow us to capture a more complete picture of the drug's pharmacokinetics. Figure 5 explores the possibility of exercise as a means to extend the sweating period. Figure 5a shows the time progression panel of fava beans intake and an image of a subject engaging in ergometer cycling. The representative pharmacokinetic profiles of sweat levodopa for three different subjects are included. In each trial, the subject consumes 450 grams of fava beans and exercises on a stationary ergometer. Each subject exercises for multiple trials and the cumulative result is shown in Figure 5b, with the averaged time of peak concentration for subject 1, 2 and 3 being 44 ± 20 minutes, 42 ± 26 minutes and 67 ± 14 minutes. It is worth noting that Figure 4a and Subject 1 of Figure 5a correspond to the same subject. The results from iontophoresis and exercise sweat show similar time of peak concentration (47 minutes versus 50 minutes). The set of on-body studies are compared to the case where no fava beans are consumed, which demonstrates almost zero concentration of levodopa (Supporting Information Figure S4). The on-body experiments demonstrate the novelties and feasibilities of the wearable *s*-band for noninvasive and continuous monitoring of levodopa's dynamic metabolic rate. We envision that this sensor platform can enable clinical understanding of xenobiotic metabolisms and dosage optimizations.

In summary, dendritic growth, enzyme immobilization and stabilizing film are seamlessly incorporated to improve the robustness and stability of the electrochemical sensor. We have also demonstrated the application of the *s*-band for prolonged, continuous and noninvasive drug monitoring in human subjects after fava beans intake. Through analyzing sweat generated via iontophoresis and physical activities, the metabolism of the drug can be tracked in real-time to allow for dosage optimization. Future directions include investigating pharmacodynamics between drugs, lengthening iontophoresis sweating duration and improving electrode lifetime upon repeated use. We envision that the wearable *s*-band can be leveraged to study the intrinsically complex drug profiles, optimize drug dosages to regulate Parkinsonian behaviors in patients and integrate with drug delivery systems. This platform serves as a pathway towards drug management for increasingly personalized, point-of-care medicine for the future.

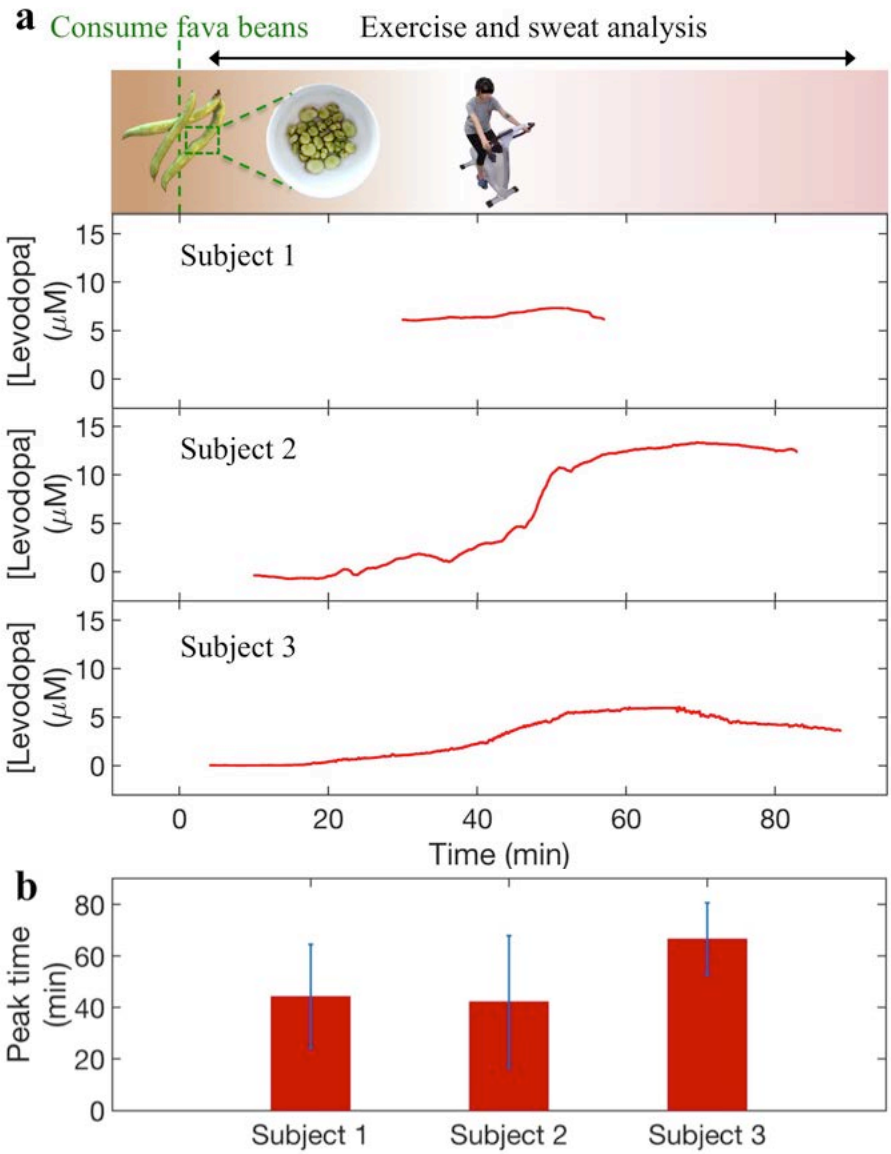

Figure 5. Levodopa monitoring via exercise induced sweat. (a) Cycling and sweat analysis. Examples of sweat levodopa concentrations for three different subjects after they consume 450 mg of fava beans. (b) Averaged time of peak levodopa concentration for three different subjects across multiple exercise trials. (Reprinted with permission from American Chemical Society).

3.5 References

(1) Piccini, P.; Brooks, D. J.; Björklund, A.; Gunn, R. N.; Grasby, P. M.; Rimoldi, O.; Brundin, P.; Hagell, P.; Rehncrona, S.; Widner, H.; Lindvall, O. Dopamine Release from Nigral Transplants Visualized in Vivo in a Parkinson's Patient. *Nat. Neurosci*. **1999**, *2*, 1137-1140.

(2) Kravitz, A. V.; Freeze, B. S.; Parker, P. R. L.; Kay, K.; Thwin, M. T.; Deisseroth, K.; Kreitzer, A. C. Regulation of Parkinsonian Motor Behaviours by Optogenetic Control of Basal Ganglia Circuitry. *Nature* **2010**, *466*, 622-626.

(3) Garnett, E. S.; Firnau, G.; Nahmias, C. Dopamine Visualized in the Basal Ganglia of Living Man. *Nature* **1983**, *305*, 137-138.

(4) Kortekaas, R.; Leenders, K. L.; van Oostrom, J. C. H.; Vaalburg, W.; Bart, J.; Willemsen, A. T. M.; Hendrikse, N. H. Blood-brain Barrier Dysfunction in Parkinsonian Midbrain in Vivo. *Ann. Neurol*. **2005**, *57*, 176-179.

(5) van Kessel, S. P.; Frye, A. K.; El-Gendy, A. O.; Castejon, M.; Keshavarzian, A.; van Dijk, G.; El Aidy, S. Gut Bacterial Tyrosine Decarboxylases Restrict Levels of Levodopa in the Treatment of Parkinson's Disease. *Nat. Commun*. **2019**, *10*, 310.

(6) Frankel, J. P.; Kempster, P. A.; Bovingdon, M.; Webster, R.; Lees, A. J.; Stern, G. M. Levodopa Peripheral Pharmacokinetics and Duration of Motor Response in Parkinson's Disease. *J. Neurol. Neurosurg. Psychiatry* **1989**, *52*, 1063-1067.

(7) Cotzias, G. C.; Van Woert, M. H.; Schiffer, L. M. Aromatic Amino Acids and Modification of Parkinsonism. *N. Engl. J. Med.* **1967**, *276*, 374-379.

(8) Deleu, D.; Jacob, P.; Chand, P.; Sarre, S.; Colwell, A. Effects of Caffeine on Levodopa Pharmacokinetics and Pharmacodynamics in Parkinson Disease. *Neurology* **2006**, *67*, 897-899.

(9) Haaxma, C. A.; Bloem, B. R.; Borm, G. F.; Oyen, W. J. G.; Leenders, K. L.; Eshuis, S.; Booij, J.; Dluzen, D. E.; Horstink, M. W. I. M. Gender Differences in Parkinson's Disease. *J. Neurol. Neurosurg. Psychiatry* **2007**, *78*, 819-824.

(10) Sossi, V.; de la Fuente-Fernández, R.; Schulzer, M.; Adams, J.; Stoessl, J. Age-related Differences in Levodopa Dynamics in Parkinson's: Implications for Motor Complications. *Brain* **2006**, *129*, 1050-1058.

(11) Crevoisier, C.; Zerr, P.; Calvi-Gries, F.; Nilsen, T. Effects of Food on the Pharmacokinetics of Levodopa in a Dual-release Formulation. *Eur. J. Pharm. Biopharm*. **2003**, *55*, 71-76.

(12) Svenningsson, P.; Rosenblad, C.; af Edholm Arvidsson, K.; Wictorin, K.; Keywood, C.; Shankar, B.; Lowe, D. A.; Björklund, A.; Widner, H. Eltoprazine Counteracts L-DOPA-induced Dyskinesias in Parkinson's Disease: a Dose-finding Study. *Brain* **2015**, *138*, 963-973.

(13) Bézard, E.; Ferry, S.; Mach, U.; Stark, H.; Leriche, L.; Boraud, T.; Gross, C.; Sokoloff, P. Attenuation of Levodopa-induced Dyskinesia by Normalizing Dopamine D3 Receptor Function. *Nat. Med*. **2003**, *9*, 762-767.

(14) Picconi, B.; Centonze, D.; Håkansson, K.; Bernardi, G.; Greengard, P.; Fisone, G.; Cenci, M. A.; Calabresi, P. Loss of Bidirectional Striatal Synaptic Plasticity in L-DOPA-induced Dyskinesia. *Nat. Neurosci*. **2003**, *6*, 501-506.

(15) Senek, M.; Aquilonius, S.-M.; Askmark, H.; Bergquist, F.; Constantinescu, R.; Ericsson, A.; Lycke, S.; Medvedev, A.; Memedi, M.; Ohlsson, F.; Spira, J.; Westin, J.; Nyholm, D. Levodopa/Carbidopa Microtablets in Parkinson's Disease: a Study of Pharmacokinetics and Blinded Motor Assessment. *Eur. J. Clin. Pharmacol*. **2017**, *73*, 563-571.

(16) Harder, S.; Baas, H.; Rietbrock, S. Concentration-effect Relationship of Levodopa in Patients with Parkinson's Disease. *Clin. Pharmacokinet*. **1995**, *29*, 243-256.

(17) Nyholm, D.; Lewander, T.; Gomes-Trolin, C.; Bäckström, T.; Panagiotidis, G.; Ehrnebo, M.; Nyström, C.; Aquilonius, S.-M. Pharmacokinetics of Levodopa/Carbidopa Microtablets versus Levodopa/Benserazide and Levodopa/Carbidopa in Healthy Volunteers. *Clin. Neuropharmacol*. **2012**, *35*, 111-117.

(18) Rabey, J. M.; Vered, Y.; Shabtai, H.; Graff, E; Korczyn, A. D. Improvement of Parkinsonian Features Correlate with High Plasma Levodopa Values after Broad

Bean (Vicia Faba) Consumption. *J. Neurol. Neurosurg. Psychiatry* **1992**, *55*, 725-727.

(19) Tsunoda, M.; Hirayama, M.; Tsuda, T.; Ohno, K. Noninvasive Monitoring of Plasma L-dopa Concentrations Using Sweat Samples in Parkinson's Disease. *Clin. Chim. Acta* **2015**, *442*, 52-55.

(20) Kovacs, E. M. R.; Stegen, J. H. C. H.; Brouns, F. Effect of Caffeinated Drinks on Substrate Metabolism, Caffeine Excretion, and Performance. *J. Appl. Physiol.* **1998**, *85*, 709-715.

(21) Birkett, D. J.; Miners, J. O. Caffeine Renal Clearance and Urine Caffeine Concentrations during Steady State Dosing. Implications for Monitoring Caffeine Intake during Sports Events. *Br. J. Clin. Pharmacol.* **1991**, *31*, 405-408.

(22) Kintz, P.; Henrich, A.; Cirimele, V.; Ludes, B. *J. Chromatogr. B.* Nicotine Monitoring in Sweat with a Sweat Patch. **1998**, *705*, 357-361.

(23) Movlaee, K.; Beitollahi, H.; Ganjali, M. R.; Norouzi, P. Electrochemical Platform for Simultaneous Determination of Levodopa, Acetaminophen and Tyrosine Using a Graphene and Ferrocene Modified Carbon Paste Electrode. *Microchim. Acta* **2017**, *184*, 3281-3289.

(24) Yue, H. Y.; Zhang, H.; Huang, S.; Lin, X. Y.; Gao, X.; Chang, J.; Yao, L. H.; Guo, E. J. Synthesis of ZnO Nanowire Arrays/3D Graphene Foam and Application for Determination of Levodopa in the Presence of Uric Acid. *Biosens. Bioelectron.* **2017**, *89*, 592-597.

(25) Thieme, D.; Rautenberg, C.; Grosse, J.; Schoenfelder, M. Significant Increase of Salivary Testosterone Levels after Single Therapeutic Transdermal Administration of Testosterone: Suitability as a Potential Screening Parameter in Doping Control. *Drug Test Anal.* **2013**, *5*, 819-825.

(26) Cone, E. J.; Hillsgrove, M. J.; Jenkins, A. J.; Keenan, R. M.; Darwin, W. D. Sweat Testing for Heroin, Cocaine, and Metabolites. *J. Anal. Toxicol.* **1994**, *18*, 298-305.

(27) Koh. A.; Kang, D.; Xue, Y.; Lee, S.; Pielak, R. M.; Kim, J.; Hwang, T.; Min, S.; Banks, A.; Bastien, P.; Manco, M. C.; Wang, L.; Ammann, K. R.; Jang, K.-I.; Won, P.; Han, S.; Ghaffari, R.; Paik, U.; Slepian, M. J.; Balooch, G.; Huang, Y.;

Rogers, J. A. A Soft, Wearable Microfluidic Device for the Capture, Storage, and Colorimetric Sensing of Sweat. *Sci. Transl. Med.* **2016**, *8*, 366ra165.

(28) Matzeu, G.; Fay, C.; Vaillant, A.; Coyle, S.; Diamond, D. A Wearable Device for Monitoring Sweat Rates via Image Analysis. *IEEE Trans. Biomed. Eng*. **2016**, *63*, 1672-1680.

(29) Tai, L.-C.; Gao, W.; Chao, M.; Bariya, M.; Ngo, Q. P.; Shahpar, Z.; Nyein, H. Y. Y.; Park, H.; Sun, J.; Jung, Y.; Wu, E.; Fahad, H. M.; Lien, D.-H.; Ota, H.; Cho, G.; Javey, A. Methylxanthine Drug Monitoring with Wearable Sweat Sensors. *Adv. Mater*. **2018**, *30*, 1707442.

(30) Gao, W.; Emaminejad, S.; Nyein, H. Y. Y.; Challa, S.; Chen, K.; Peck, A.; Fahad, H. M.; Ota, H.; Shiraki, H.; Kiriya, D.; Lien, D.-H.; Brooks, G. A.; Davis, R. W.; Javey, A. Fully Integrated Wearable Sensor Arrays for Multiplexed *in Situ* Perspiration Analysis. *Nature* **2016**, *529*, 509−514.

(31) Emaminejad, S.; Gao, W.; Wu, E.; Davies, Z. A.; Yin Yin Nyein, H.; Challa, S.; Ryan, S. P.; Fahad, H. M.; Chen, K.; Shahpar, Z.; Talebi, S.; Milla, C.; Javey, A.; Davis, R. W. Autonomous Sweat Extraction and Analysis Applied to Cystic Fibrosis and Glucose Monitoring Using a Fully Integrated Wearable Platform. *Proc. Natl. Acad. Sci. U. S. A.* **2017**, *114*, 4625−4630.

(32) Kim. J.; Jeerapan, I.; Imani, S.; Cho, T. N.; Bandodkar, A.; Cinti, S.; Mercier, P. P.; Wang, J. Non-invasive Alcohol Monitoring Using a Wearable Tattoo-based Iontophoretic-biosensing System. *ACS Sens.* **2016**, *1*, 1011–1019.

(33) Krishnan, S. R.; Ray, T. R.; Ayer, A. B.; Ma, Y.; Gutruf, P.; Lee, K.; Lee, J. Y.; Wei, C.; Feng, X.; Ng, B.; Abecassis, Z. A.; Murthy, N.; Stankiewicz, I.; Freudman, J.; Stillman, J.; Kim, N.; Young, G.; Goudeseune, C.; Ciraldo, J.; Tate, M.; Huang, Y.; Potts, M.; Rogers, J. A. Epidermal Electronics for Noninvasive, Wireless, Quantitative Assessment of Ventricular Shunt Function in Patients with Hydrocephalus. *Sci. Transl. Med*. **2018**, *10*, eaat8437.

(34) Takei, K.; Takahashi, T.; Ho, J. C.; Ko, H.; Gillies, A. G.; Leu, P. W.; Fearing, R. S.; Javey, A. Nanowire Active Matrix Circuitry for Low-voltage Macro-scale Artificial Skin. *Nat. Mater*. **2010**, *9*, 821–826.

(35) Ota, H.; Chen, K.; Lin, Y.; Kiriya, D.; Shiraki, H.; Yu, Z.; Ha, T.-J.; Javey, A. Highly-deformable Liquid-state Heterojunction Sensors. *Nat. Commun* **2014**, *5*,

5032.

(36) Boutry, C. M.; Beker, L.; Kaizawa, Y.; Vassos, C.; Tran, H.; Hinckley, A. C.; Pfattner, R.; Niu, S.; Li, J.; Claverie, J.; Wang, Z.; Chang, J.; Fox, P. M.; Bao, Z. Biodegradable and Flexible Arterial-pulse Sensor for the Wireless Monitoring of Blood Flow. *Nat. Biomed. Eng*. **2019**, *3*, 47-57.

(37) Brunetti, B.; Valdés-Ramírez, G.; Litvan, I.; Wang, J. A Disposable Electrochemical Biosensor for L-DOPA Determination in Undiluted Human Serum. *Electrochem. Commun*. **2014**, *48*, 28-31.

(38) Lin, Y.; Gao, Y.; Fan, Z. Printable Fabrication of Nanocoral-structured Electrodes for High-performance Flexible and Planar Supercapacitor with Artistic Design. *Adv. Mater* **2017**, *29*, 1701736.

(39) Wang, S.; Wu, Y.; Gu, Y.; Li, T.; Luo, H.; Li, L.-H.; Bai, Y.; Li, L.; Liu, L.; Cao, Y.; Ding, H.; Zhang, T. Wearable Sweatband Sensor Platform Based on Gold Nanodendrite Array as Efficient Solid Contact of Ion-Selective Electrode. *Anal. Chem*. **2017**, *89*, 10224-10231.

(40) Dempsey, E.; Diamond, D.; Collier, A. Development of a Biosensor for Endocrine Disrupting Compounds Based on Tyrosinase Entrapped within a Poly(thionine) Film. *Biosens. Bioelectron*. **2004**, *20*, 367-377.

(41) Qi, L.; Thomas, E.; White, S. H.; Smith, S. K.; Lee, C. A.; Wilson, L. R.; Sombers, L. A. Unmasking the Effects of L-DOPA on Rapid Dopamine Signaling with an Improved Approach for Nafion Coating Carbon-fiber Microelectrodes. *Anal. Chem*. **2016**, *88*, 8129-8136.

(42) Ye, W.; Yan, J.; Ye, Q.; Zhou, F. Template-free and Direct Electrochemical Deposition of Hierarchical Dendritic Gold Microstructures: Growth and Their Multiple Applications. *J. Phys. Chem. C* **2010**, *114*, 15617-15624.

3.6 Appendix

Sensor fabrication. The flexible electrodes were fabricated on PET substrates via photolithography and evaporation. The electrodes were patterned through photolithography with positive photoresist (Shipley Microposit S1818) and electron-beam evaporation of Cr (30 nm) and Au (50 nm). Afterwards, lift-off in acetone solution was performed. Au nano-dendrites were grown on top of the electrodes with a Gamry Electrochemical Potentiostat (signal type: square wave; signal frequency: 50 Hz; amplitude: 1V; DC offset -1 V; cycles: 6000) and chloroauric acid solution (mixture of 50 mM $AuCl_3$ and 50 mM HCl). The precursor concentration will affect the morphology and length of the nanostructures; while increasing the deposition time will normally increase the length of the nanostructures.[42] The 6000 cycles (120 seconds) of Au deposition were chosen because the resulting functionalized electrode shows the largest current change upon the addition of 10 μM of levodopa, as shown in Supporting Information Figure S3. The electrodes were immediately cleaned with deionized water and left in room temperature for 2 hours for drying. On top of the Au nano-dendrites, 0.25 mM of thionin acetate salt (Sigma-Aldrich) was deposited electrochemically with CV (initial potential: -0.6 V; final potential: 0.1 V; scan rate: 0.1 V/s; segment: 40). The electrodes were then left in room temperature for 2 hours. Subsequently, a mixture of enzyme and crosslinker solution was drop-casted on top of the electrodes (2.5 μL). The solution was prepared by mixing tyrosinase (Sigma-Aldrich. 1 mg) with 2% glutaraldehyde (Sigma-Aldrich. 0.866 μL) in PBS (66.6 μL). The electrodes were left in room temperature for 12 hours. Finally, Nafion 117 (Sigma Aldrich. 1 μL) was drop-casted on top of the electrodes, and the electrodes were left in room temperature for 2 hours. For the reference electrodes, Ag/AgCl paste was painted on top of the Au electrodes and left in room temperature for 12 hours.

Sensor characterization and calibration. The functionalized electrodes were characterized electrochemically using CHI 1230C potentiostat (CH Instrument) in CV and amperometric measurements. The CV and amperometric responses corresponding to different concentrations of levodopa were subsequently evaluated. The interference test involved the addition of various biomolecules at the physiologically relevant concentrations. In Figure 2, the functionalized working electrodes were characterized with commercial Ag/AgCl reference electrode in PBS. In Figure 3, on-body functionalized electrode arrays, including functionalized working electrodes, Ag/AgCl pasted reference electrodes and Au counter electrodes (all on PET substrate), were characterized in sweat solutions collected from the exercise trials.

Iontophoresis sweat analysis. Iontophoresis was conducted by gently mounting pilocarpine hydrogel (ELITechGroup SS-023 Pilogel) on a subject's wrist for 5 minutes at 1 mA DC current (ELITechGroup Model 3700 Webster Sweat Inducer). During in situ evaluation, electrode arrays were placed conformal to the skin and connected to the CHI 1230C potentiostat. The on-body sweat analysis of human subjects was approved by the institutional review board (CPHS 2016-06-8853) at the University of California, Berkeley. The on-body sweat analyses were processed with MATLAB's Hampel and Smooth functions for noise reduction.

Exercise sweat analysis. The subjects engaged in stationary cycling on an ergometer (Gold's Gym 290C Upright Cycle Trainer) at a biking power of 100 W. The electrode arrays were calibrated and tested with the same method as that in the iontophoresis sweat analysis section. The continuous data is plotted when the sensor starts to respond in sweat solutions. This corresponds to the time when we observe obvious sweating on the subject and sufficient accumulation of sweat around the sensor. The uncertainty for the time of peak concentration in Figure 5b was defined as the standard deviation of all the exercise trials for the same subject. One trial was performed for subject 3, and the uncertainty was estimated from the slope (concentration/time) around the proximity of the pharmacokinetic peak and the sensor drift (uncertainty in concentration).

Food intake. Fava beans were purchased from a local community market (Berkeley Bowl). 250 g of fava beans consumption is equivalent to about 125 mg of levodopa intake.[18] The sandwich was a 12-inch Italian B. M. T. sandwich (Subway®). The fava beans' seeds were taken out from the bean pods and cooked in boiling water for 20 minutes prior to consumption.

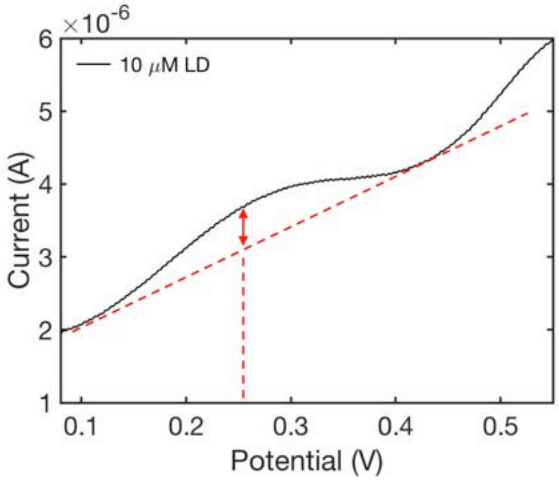

Figure S1. Method of determining the peak potential. A tangent line is drawn at the proximity of the CV peak, and the potential corresponding to the largest peak height can be traced via the vertical dotted line. (Reprinted with permission from American Chemical Society).

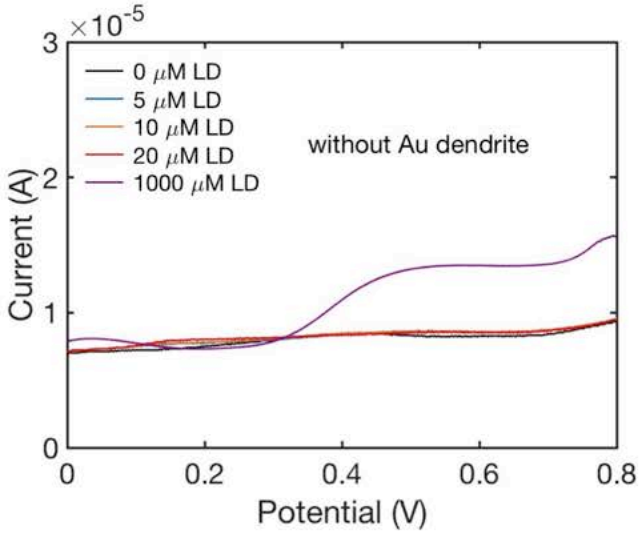

Figure S2. CV of levodopa dissolved in PBS tested with bare Au working electrode, commercial Ag/AgCl reference electrode, and Pt counter electrode. (Reprinted with permission from American Chemical Society).

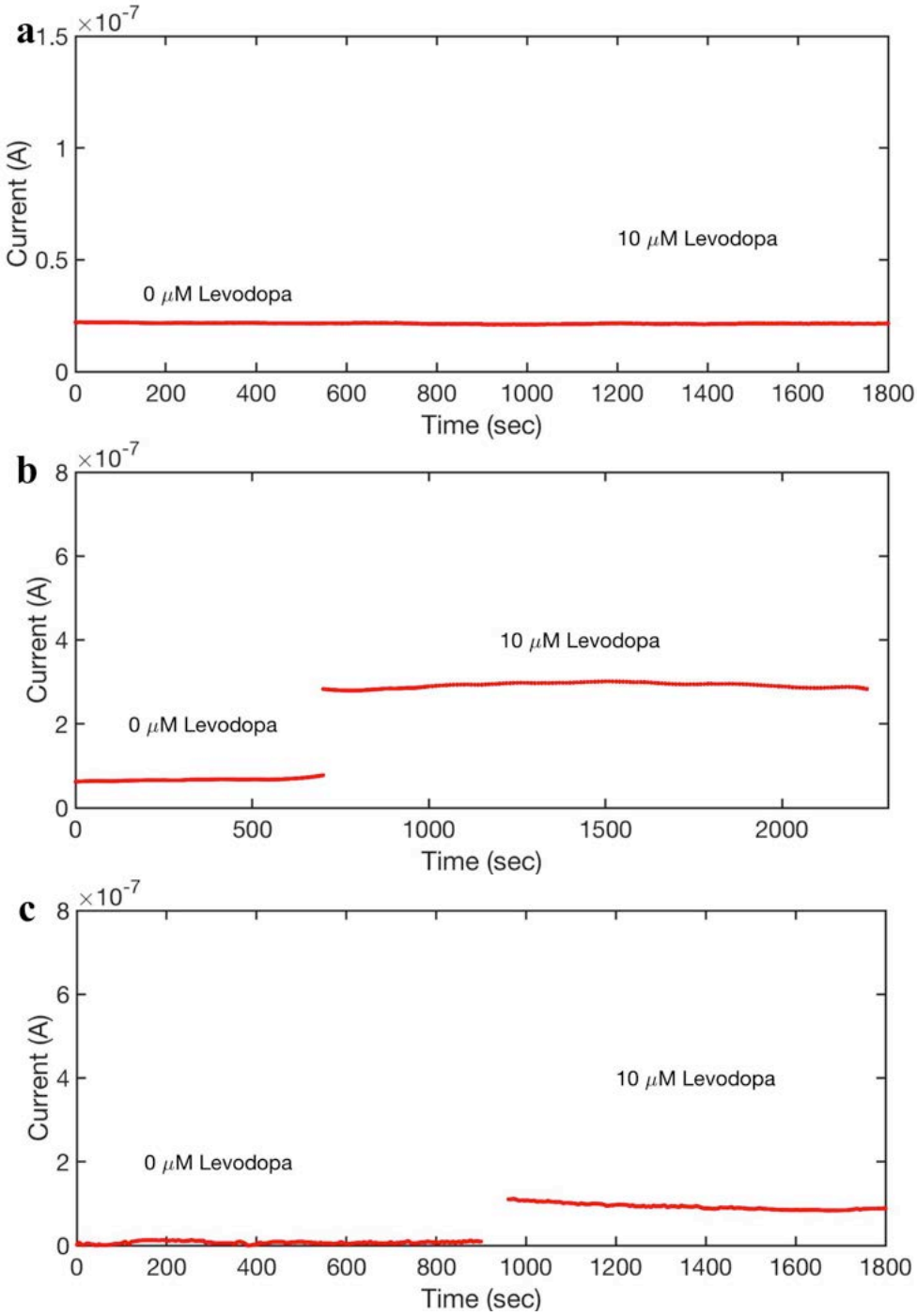

Figure S3. Long-term amperometric test for the functionalized working electrode for Au dendrite deposition time of (a) 60 seconds, (b) 120 seconds and (c) 240 seconds. (Reprinted with permission from American Chemical Society).

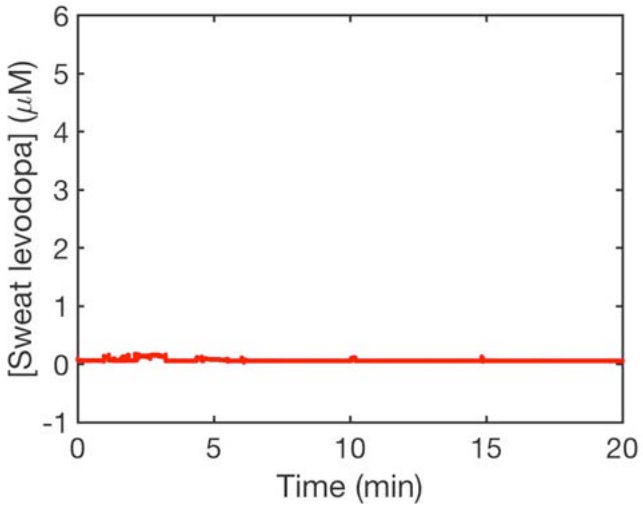

Figure S4. Levodopa sensor response with iontophoresis-induced sweat without fava beans consumption. The sweat levodopa concentration is almost zero compared to the case with fava beans consumption. (Reprinted with permission from American Chemical Society).

Chapter 4 Nicotine Monitoring with Wearable Sweat Sensors

The following chapter has been previously written in a similar format.

4.1 Introduction to Secondhand Smoke

Tobacco exposure is a leading modern-day epidemic that has claimed more than eight million lives worldwide every year from direct tobacco use and indirect exposure to secondhand smoke.[1] These statistics convey the broad scope of people affected by smoking and the need to spearhead effective measures against smoke pollution. The adverse physiological and psychological side effects of ingredients in cigarettes can lead to sleep disorders, cardiovascular diseases, addictions, diabetes, and respiratory dysfunctions.[1-6] Therefore, tobacco smoke that permeates into various environments presents a serious public health threat that merits careful attention. The cumulative exposure to secondhand smoke in public spaces and private environments can be hard to quantify, which leads to the underestimation of irreversible health consequences on nonsmoking individuals.[7] Therefore, a tobacco monitoring device is necessary to properly evaluate the scope of health risks among nonsmoking populations. The conventional technique to detect tobacco smoke mounts a sensor at a fixed location, which lacks the flexibility to determine smoke exposure on specific individuals and offer personalized alerts.[8] Commercially available tobacco test strips allow users to analyze urine and saliva specimens to monitor nicotine exposure at separate time points.[9] However, a test strip's inability for continuous monitoring and inconvenient processing steps make it practically challenging to capture a complete picture of an individual's exposure to tobacco, and thus making efforts of tailoring preventive strategies difficult. To address the abovementioned obstacles, we present a wearable sweat band (*s*-band) for nicotine monitoring to bridge the technological gap between mounted tobacco detectors and discrete nicotine testing strips. In this work, sweat is distinctively chosen as the sensing bio-fluid because of its abundance in biomolecules and its great accessibility.[10-17] Nicotine is selected as an attractive target due to its presence in nearly all tobacco products.[20] Like many xenobiotic biomolecules, nicotine has been demonstrated to excrete in sweat, with its concentrations positively correlated with smoking.[17-19,21] Additionally, under normal smoking

conditions, sweat nicotine concentration is expected to reach up to several micro-molars, which is within the detectable range with existing nicotine sensing technologies.[17,21-25] This intimate connection between individuals' exposure to nicotine and their sweat nicotine levels provides us the framework to design a wearable *s*-band for nicotine monitoring. An electrochemical technique is chosen for sensor development because of its advantages for high sensitivity, good selectivity, compatibility with electronics, and low costs.[10-16] Our approach addresses the shortcomings of the current smoke monitoring devices and paves a way to continuous, real-time, and on-site secondhand smoke monitoring.

4.2 Device Background and Sensing Mechanism

Figure 1a shows the nicotine *s*-band consisted of a flexible electrode array connected to a compact printed circuit board. During an on-body use, the *s*-band is worn on the subject's forearm to detect the level of nicotine in human sweat after nicotine inhalation. The cross sectional layers of the electrode array are shown in Figure 1b. On a polyethylene terephthalate (PET) film, a gold working electrode is grown with gold nano-dendrites and modified with cytochrome P450 2B6 (CYP2B6), a nicotine oxidizing enzyme.[26-29] A silver/silver chloride reference electrode and a gold counter electrode are also integrated. Figure 1c shows a zoom-in view of the functionalized working electrode. Gold nano-dendrites are directly grown on the gold electrode, and a self-assembled monolayer of 11-mercaptoundecanoic acid (MUA) is coated on top.[30,31] The MUA then immobilizes the enzyme by covalently bonding with CYP2B6.[32-34] The successful addition of each layer is supported by the electrochemical impedance spectroscopy, shown in Figure S1.

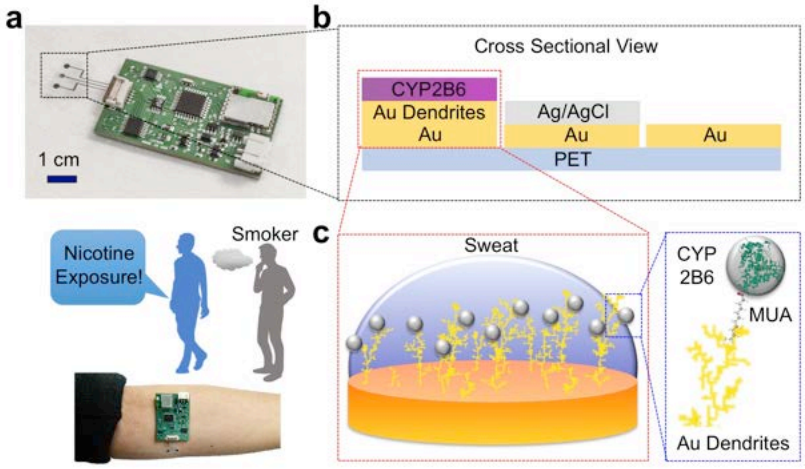

Figure 1. The design and application of the *s*-band. (a) Optical image of a nicotine *s*-band and a schematic showing the application of the wearable device on monitoring secondhand smoke. (b) A cross-sectional illustration of the flexible sensor patch, which consists of a functionalized working electrode modified with CYP2B6 enzyme, a reference electrode pasted with silver/silver chloride, and a counter electrode. (c) Zoom-in schematics of the functionalized working electrode, which has gold nano-dendrites grown on top of the gold substrate. The nano-dendrites are connected to CYP2B6, a nicotine oxidizing enzyme, via a self-assembled monolayer of 11-mercaptoundecanoic acid (MUA). (Reprinted with permission from American Chemical Society).

4.3 Sensor Characterization

The gold nano-dendritic structure of the functionalized working electrode was captured with a scanning electron microscope (SEM), shown in Figure 2a. The gold nano-dendrites increase the surface area of the electrode to improve the sensitivity and stability of the sensor.[13,30] Figure 2b shows the oxidation peak from cyclic voltammetry (CV) of the functionalized electrode in phosphate-buffered saline (PBS) solution, with the subsequent addition of nicotine (0 – 30 µM). The oxidation peak increases in its height with increasing concentration of nicotine and is centered at 0.8 V, the potential chosen for amperometric testing.[22-25] For the purpose of comparison, Figure S2 shows nicotine's distinct peak relative to other xenobiotic molecules such as caffeine and levodopa. Figure 2c shows a representative plot of the amperometric response of the functionalized electrode to nicotine, and its corresponding current-to-concentration calibration curve is shown in Figure 2d. The sensitivity is calculated to be 4.3 nA/µM, which is on par with the state-of-the-art nicotine sensors.[22,23] Figure 2e shows a histogram plot of the

sensor-to-sensor variation in terms of their sensitivities. The standard deviation is found to be 1.4 nA/μM, which contributes up to 30 % of deviation that dominates the linear calibration curve's uncertainty. For a high sweat nicotine level of 5 μM, this translates to about 1.6 μM of uncertainty. The effects of pH and temperature can potentially influence the performance of enzymatic-based sensors.[11] Figure 2f shows the functionalized electrode's response to varying degrees of pH, prepared using McIlvaine buffer. The range of pH (5 – 7) is selected in the physiologically relevant range of human sweat, and the corresponding sensitivities have a standard deviation of 0.9 nA/μM, which is within the standard deviation calculated from sensor-to-sensor variations.[11] The effect of the temperature is demonstrated in Figure 2g, where the functionalized electrode is first spiked with 5 μM of nicotine, followed by gradually increasing the temperature from 20 °C to 40 °C. The result shows the sensitivity to temperature is 2.2 nA/°C, which is used to calibrate the amperometric readings prior to conversion into nicotine concentrations. The functionalized electrode's responses to interferents are tested in Figure 2h, with the addition of common biomolecules such as glucose (100 μM), ascorbic acid (10 μM), uric acid (20 μM), and caffeine (10 μM). The interferences are found to contribute to about ± 1 μM of uncertainty when compared to the sensor's response to nicotine.

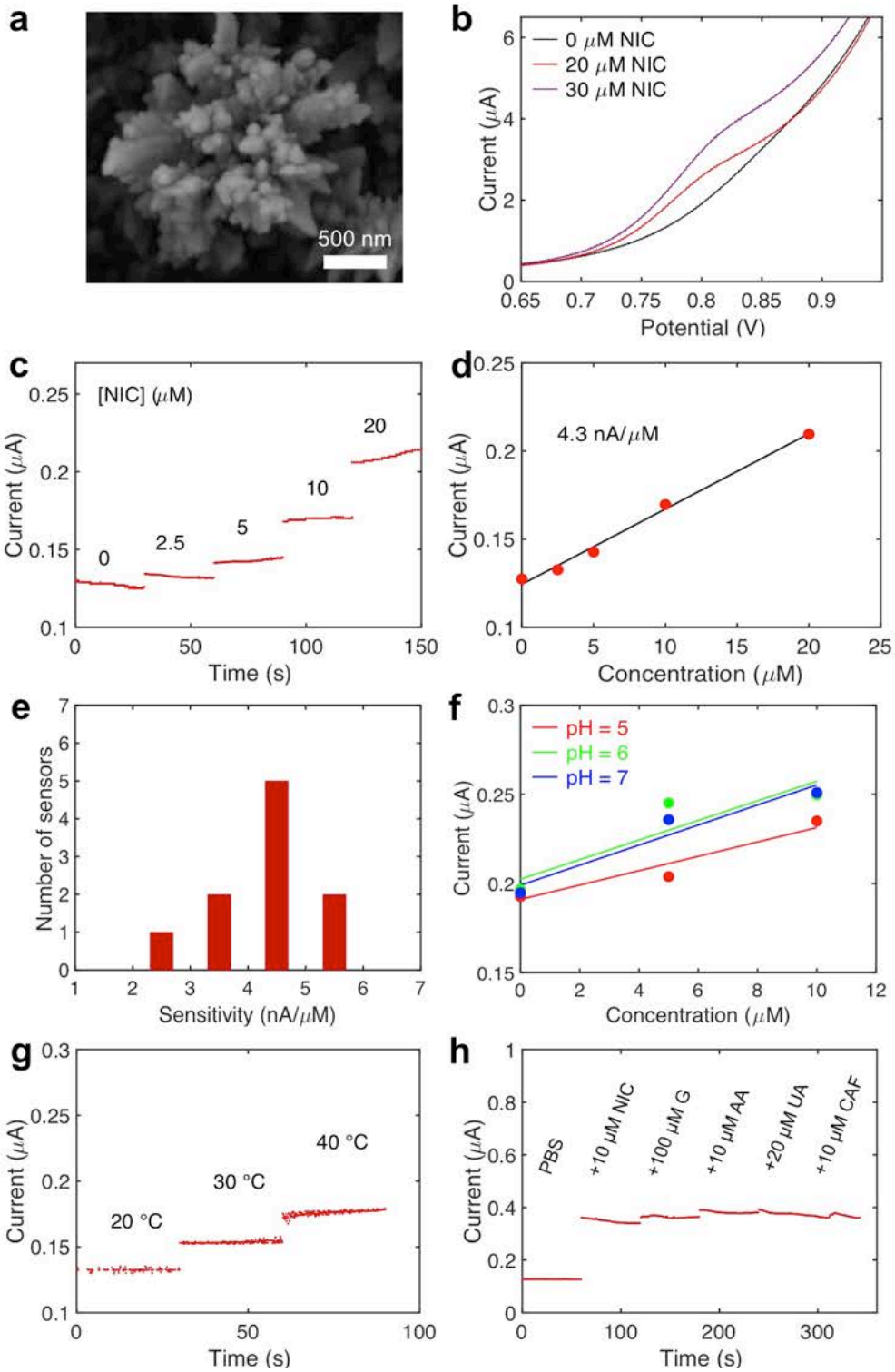

Figure 2. Characterization of the functionalized working electrode in PBS. (a) SEM image of the gold nano-dendrites. (b) Zoom-in view of a CV of nicotine (NIC) dissolved in PBS. (c) The amperometric response of nicotine dissolved in PBS and (d) linear relationship of the amperometric current and nicotine

concentration. (e) Sensor-to-sensor variations in terms of sensitivities. (f) The effect of pH on sensor sensitivities. (g) The effect of temperature on the amperometric response. (h) The effect of potential interferents, such as glucose (G), ascorbic acid (AA), uric acid (UA), and caffeine (CAF), on the amperometric response. (Reprinted with permission from American Chemical Society).

To characterize the sensor performance in human sweat, Figure 3 shows the functionalized electrode's response in sweat solutions. Figure 3a shows a schematic of the sensing of nicotine molecules in sweat solutions, where the CYP2B6 enzyme oxidizes nicotine into nicotine iminium ion.[26-29] Figure 3b shows the amperometric response of nicotine being oxidized at a constant applied potential of 0.8 V. By adding nicotine into the sweat solution, the Faradaic current increases gradually, and the current-to-concentration calibration is shown in Figure 3c. The sensitivity is found to be 4.4 nA/μM, which is similar to the sensitivity tested in PBS.

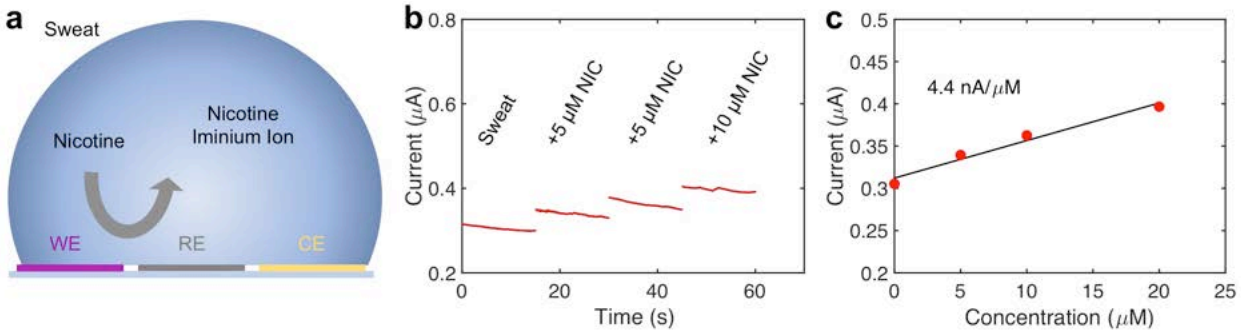

Figure 3. Characterization of the nicotine sensor in sweat solutions. (a) Sensing nicotine molecules in sweat solutions. Sweat nicotine is oxidized via CYP2B6 on the working electrode (WE) into nicotine iminium ion. The reference electrode (RE) and the counter electrode (CE) are also shown. This oxidation generates a current that is measured in terms of (b) the amperometric response to nicotine. (c) The corresponding calibration curve. (Reprinted with permission from American Chemical Society).

4.4 Sweat Analysis

Figure 4 explores the possibility of utilizing the nicotine *s*-band to detect an individual's exposure to nicotine. Both nonsmoking subjects and smokers

volunteered for this study. The subjects were permitted to generate sweat via various approaches, such as cycling, intense walking, and sports competition. Nonsmokers had no tobacco exposure, and their sweat solutions were directly analyzed after perspiration. Regular smokers started exercising within five minutes after they each smoked a standard cigarette. Their sweat solutions were similarly analyzed when they started sweating, typically five to ten minutes after the start of their exercise. Figure 4a shows the experimental design using the *s*-band for nicotine monitoring. The subjects smoked before engaging in physical activities to generate sweat. Sweat nicotine levels were then analyzed, as described in the Experimental Section. In Figure 4b, different exercise trials, including both nonsmokers and smokers, were performed to compare the sweat nicotine levels between controls and subjects exposed to nicotine. Our results show consistently low concentrations for nonsmokers, with average nicotine levels below the limit of detection. The smokers' sweat samples exhibit elevated nicotine concentrations with an average value of 4.8 μM, which is within the concentration range previously observed.[17,21] One smoker shows a low nicotine level. This is potentially due to various factors, such as metabolic rates, the amount of nicotine content in cigarettes, and the degree of nicotine inhalation during smoking. Nevertheless, on average, we observe a good distinction between the sweat nicotine concentration between the nonsmokers and smokers. This set of experiments demonstrates the potential for distinguishing the subjects' exposure to nicotine using sweat solutions. Prior to on-body trials, the nicotine sensor is tested for a long duration, as shown in Figure S3. The signal-to-noise ratio (SNR) is calculated by dividing the change in amperometric current with the addition of 5 μM nicotine (about half of the maximum observed value of sweat nicotine concentration after regular smoking) by the amplitude of current fluctuation.[17] Based on Figure S3, the SNR is calculated to be 4, which corresponds to about 1.3 μM of uncertainty due to noise. The sensor's overall drift is small, corresponding to less than 0.16 μM/min. The detection limit is then calculated by looking at the uncertainty calculated earlier due to the interference (1 μM), sensor-to-sensor variation and linear calibration (1.6 μM), noise level (1.3 μM), and sensor drift over the average duration of on-body testing (1.3 μM) and assigning the largest value. The precision of our measurement is then constrained by the detection limit of 1.6 μM.

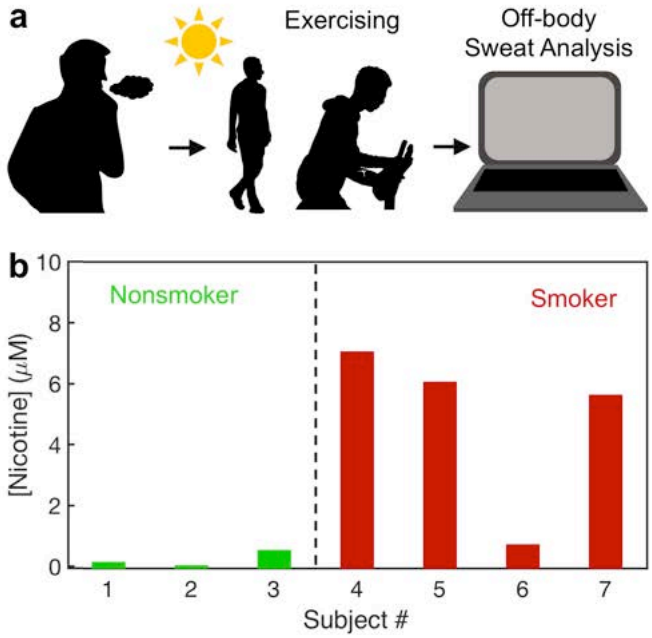

Figure 4. Nicotine monitoring via exercise-induced sweat. Sweat samples are collected after smoking (for smoking subjects) and subsequent exercise. (a) Schematics of the experiment. (b) Nicotine concentrations measured for nonsmokers and smokers. (Reprinted with permission from American Chemical Society).

In order to demonstrate the use of nicotine *s*-band for continuous nicotine monitoring, multiple subjects were recruited for sweat analysis. Figure 5a shows the experimental design with the subjects going through cycling on an ergometer. The on-body *s*-band seamlessly measures the nicotine level over time, with time zero indicating the start of sweating. Figure 5b shows the images of a subject cycling on an ergometer and a zoom-in view of the *s*-band. Two types of on-body experiments were performed. The first group includes healthy nonsmokers, and they were instructed to cycle on the ergometer for half an hour or until fatigue. As shown in Figure 5c, the nonsmokers' sweat profiles demonstrate a low nicotine concentration typically below the detection limit. Figure 5d monitors the smokers' sweat nicotine profiles. The smokers smoke one cigarette, which contains about 13 mg of nicotine, right before cycling on an ergometer.[35-37] Their sweat profiles are then analyzed to evaluate the concentrations of nicotine. The nicotine concentrations indicate an average peak level of 5.8 μM. In both smokers' profiles, the sweat nicotine concentrations increase in the beginning, which may be attributed to the absorption of nicotine that typically happens on the order of minutes. After reaching their respective peaks, we do not observe obvious variation in their nicotine concentrations. This may be attributed to nicotine's slow

metabolic decay, with the expected half-life on the order of hours.[38-40] Comparing Figure 5c and 5d, the distinctions between sweat profiles from smokers and nonsmokers show that the *s*-band can pick up the inhalation of nicotine.

In conclusion, we have demonstrated a noninvasive and wearable *s*-band capable of monitoring nicotine. Our work combines several layers of modification on the working electrode to allow for effective sensing. By integrating the physical properties of gold nano-dendrites and the chemical bonding enabled through the self-assembled monolayers, the sensor exhibits good sensitivity and stability that are essential for detecting nicotine in sweat solutions. This amenable platform can serve as a template for future sensor designs. We have also investigated the sweat nicotine concentrations between nonsmokers and smokers, as well as their nicotine profiles over time. Our observation shows that the nicotine *s*-band is capable of directly picking up nicotine levels in real-time for those inhaling cigarette smoke.

Importantly, the *s*-band overcomes the shortcomings of other commercial tobacco detectors that are limited by their lack of mobility and inability for continuous measurements. From the society's point of view, the *s*-band provides the general population an excellent device to monitor secondhand smoke and allows for effective policymaking related to smoke prevention. In tandem with existing sensor networks and big data analysis, the nicotine *s*-band can remarkably impact the healthcare industry by enriching the bioinformatics available to its users. We envision that the nicotine *s*-band's long-term monitoring capability and its application geared toward the general public will significantly expand the realm of wearable sensing technologies and chart new territories for biomedical discoveries. Further, the longitudinal and cross sectional studies enabled through the nicotine *s*-band will provide us with profound insight into various chronic and underlying pathological conditions that can be explored for preventive care and personalized medication.

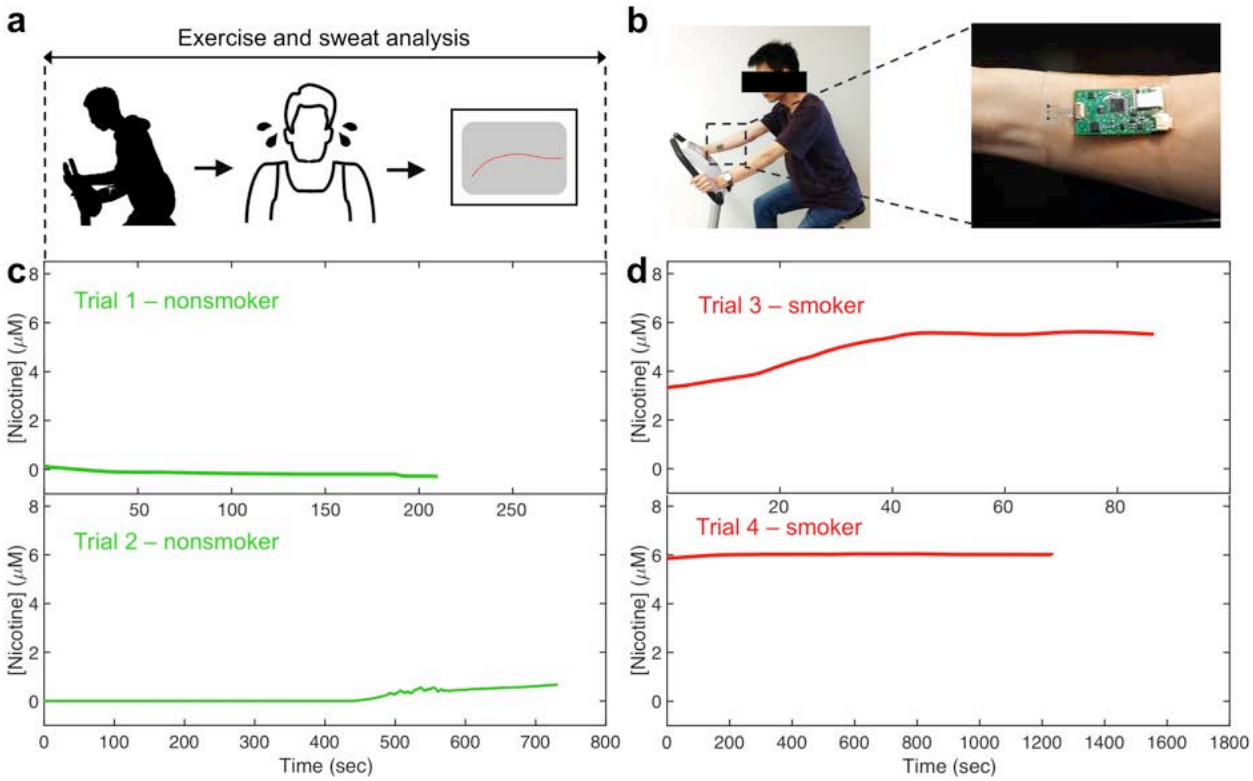

Figure 5. On-body nicotine monitoring via exercise-induced sweat. (a) Schematics of the experiment and (b) optical images of the experiment. Examples of sweat nicotine concentrations for subjects cycling on an ergometer (c) without smoking, and (d) with smoking. (Reprinted with permission from American Chemical Society).

4.5 References

(1) Beaglehole, R.; Bates, C.; Youdan, B.; Bonita, R. Nicotine without Smoke: Fighting the Tobacco Epidemic with Harm Reduction. *Lancet* **2019**, *394*, 718-720.

(2) Pullan, R. D.; Rhodes, J.; Ganesh, S.; Mani, V.; Morris, J. S.; Williams, G. T.; Newcombe, R. G.; Russell, M.; Feyerabend, C.; Thomas, G.; Sawe, U. Transdermal Nicotine for Active Ulcerative Colitis. *N. Engl. J. Med.* **1994**, *330*, 811-815.

(3) Kaufman, D. W.; Helmrich, S. P.; Rosenberg, L.; Miettinen, O. S.; Shapiro, S. Nicotine and Carbon Monoxide Content of Cigarette Smoke and the Risk of Myocardial Infarction in Young Men. *N. Engl. J. Med*. **1983**, *308*, 409-413.

(4) Duncan, A.; Heyer, M. P.; Ishikawa, M.; Caligiuri, S. P. B.; Liu, X.-A.; Chen, Z.; Micioni Di Bonaventura, M.V.; Elayouby, K. S.; Ables, J. L.; Howe, W. M.; Bali, P.; Fillinger, C.; Williams, M.; O'Connor, R. M.; Wang, Z.; Lu, Q.; Kamenecka, T. M.; Ma'ayan, A.; O'Neill, H. C.; Ibanez-Tallon, I.; Geurts, A. M.; Kenny, P. J. Habenular TCF7L2 Links Nicotine Addiction to Diabetes. *Nature* **2019**, *574*, 372–377.

(5) Honein, M. A.; Rasmussen, S. A.; Reefhuis, J.; Romitti, P. A.; Lammer, E. J.; Sun, L.; Correa, A. Maternal Smoking and Environmental Tobacco Smoke Exposure and the Risk of Orofacial Clefts. *Epidemiology* **2007**, *18*, 226-233.

(6) Popa, C. Breathing Disorders Using Photoacoustics Gas Analyzer. *J. Med. Imaging Health Inform*. **2016**, *6*, 1893–1895.

(7) Coultas, D. B.; Howard, C. A.; Peake, G. T.; Skipper, B. J.; Samet, J. M. Salivary Cotinine Levels and Involuntary Tobacco Smoke Exposure in Children and Adults in New Mexico. *Am. Rev. Respir. Dis*. **1987**, *136*, 305–309.

(8) Liu, Y.; Antwi-Boampong, S.; BelBruno, J. J.; Crane, M. A.; Tanski, S. E. Detection of Secondhand Cigarette Smoke via Nicotine Using Conductive Polymer Films. *Nicotine Tob. Res.* **2013**, *15*, 1511–1518.

(9) Achilihu, H.; Feng, J.; Wang, L.; Bernert, J. .T. Tobacco Use Classification by Inexpensive Urinary Cotinine Immunoassay Test Strips, *J. Anal Toxicol.* **2019**, *43*, 149–153.

(10) Tai, L.-C.; Gao, W.; Chao, M.; Bariya, M.; Ngo, Q. P.; Shahpar, Z.; Nyein, H. Y. Y.; Park, H.; Sun, J.; Jung, Y.; Wu, E.; Fahad, H. M.; Lien, D.-H.; Ota, H.; Cho,

G.; Javey, A. Methylxanthine Drug Monitoring with Wearable Sweat Sensors. *Adv. Mater*. **2018**, *30*, 1707442.

(11) Gao, W.; Emaminejad, S.; Nyein, H. Y. Y.; Challa, S.; Chen, K.; Peck, A.; Fahad, H. M.; Ota, H.; Shiraki, H.; Kiriya, D.; Lien, D.-H.; Brooks, G. A.; Davis, R. W.; Javey, A. Fully Integrated Wearable Sensor Arrays for Multiplexed *in Situ* Perspiration Analysis. *Nature* **2016**, *529*, 509−514.

(12) Emaminejad, S.; Gao, W.; Wu, E.; Davies, Z. A.; Yin Yin Nyein, H.; Challa, S.; Ryan, S. P.; Fahad, H. M.; Chen, K.; Shahpar, Z.; Talebi, S.; Milla, C.; Javey, A.; Davis, R. W. Autonomous Sweat Extraction and Analysis Applied to Cystic Fibrosis and Glucose Monitoring Using a Fully Integrated Wearable Platform. *Proc. Natl. Acad. Sci. U. S. A.* **2017**, *114*, 4625−4630.

(13) Tai, L.-C.; Liaw, T. S.; Lin, Y.; Nyein, H. Y. Y.; Bariya, M.; Ji, W.; Hettick, M.; Zhao, C.; Zhao, J.; Hou, L.; Yuan, Z.; Fan, Z.; Javey, A. Wearable Sweat Band for Noninvasive Levodopa Monitoring. *Nano Lett.* **2019**, *19*, 6346-6351.

(14) Nyein, H. Y. Y.; Bariya, M.; Kivimäki, L.; Uusitalo, S.; Liaw, T. S.; Jansson, E.; Ahn, C. H.; Hangasky, J. A.; Zhao, J.; Lin, Y.; Happonen, T.; Chao, M.; Liedert, C.; Zhao, Y.; Tai, L.-C.; Hiltunen, J.; Javey, A. Regional and Correlative Sweat Analysis Using High-throughput Microfluidic Sensing Patches Toward Decoding Sweat. *Sci. Adv*. **2019**, *5*, No. eaaw9906.

(15) Kim, J.; Jeerapan, I.; Imani, S.; Cho, T. N.; Bandodkar, A.; Cinti, S.; Mercier, P. P.; Wang, J. Noninvasive Alcohol Monitoring Using a Wearable Tattoo-Based Iontophoretic-Biosensing System. *ACS Sens*. **2016**, *1*, 1011−1019.

(16) Krishnan, S. R.; Ray, T. R.; Ayer, A. B.; Ma, Y.; Gutruf, P.; Lee, K.; Lee, J. Y.; Wei, C.; Feng, X.; Ng, B.; Abecassis, Z. A.; Murthy, N.; Stankiewicz, I.; Freudman, J.; Stillman, J.; Kim, N.; Young, G.; Goudeseune, C.; Ciraldo, J.; Tate, M.; Huang, Y.; Potts, M.; Rogers, J. A. Epidermal Electronics for Noninvasive, Wireless, Quantitative Assessment of Ventricular Shunt Function in Patients with Hydrocephalus. *Sci. Transl. Med.* **2018**, *10*, No. eaat8437.

(17) Kintz, P.; Henrich, A.; Cirimele, V.; Ludes, B. Nicotine Monitoring in Sweat with a Sweat Patch. *J. Chromatogr. B: Biomed. Sci. Appl*. **1998**, *705*, 357-361.

(18) Tsunoda, M.; Hirayama, M.; Tsuda, T.; Ohno, K. Noninvasive Monitoring of Plasma L-dopa Concentrations Using Sweat Samples in Parkinson's Disease. *Clin. Chim. Acta* **2015**, *442*, 52−55.

(19) Kovacs, E. M. R.; Stegen, J. H. C. H.; Brouns, F. Effect of Caffeinated Drinks on Substrate Metabolism, Caffeine Excretion, and Performance. *J. Appl. Physiol*. **1998**, *85*, 709−715.

(20) Stanfill, S. B.; Connolly, G. N.; Zhang, L.; Jia, L. T.; Henningfield, J. E.; Richter, P.; Lawler, T. S.; Ayo-Yusuf, O. A.; Ashley, D. L.; Watson, C. H. Global surveillance of oral tobacco products: total nicotine, unionised nicotine and tobacco-specific N-nitrosamines. *Tob. Control* **2011**, *20*, No. e2.

(21) Henningfield, J. E.; Stapleton, J. M.; Benowitz, N. L.; Grayson, R. F.; London, E. D. Higher Levels of Nicotine in Arterial than in Venous Blood after Cigarette Smoking. *Drug Alcohol Depend*. **1993**, *33*, 23-29.

(22) Jing, Y.; Yuan, X.; Yuan, Q.; He, K.; Liu, Y.; Lu, P.; Li, H.; Li, B.; Zhan, H.; Li, G. Determination of Nicotine in Tobacco Products Based on Mussel-inspired Reduced Graphene Oxide-supported Gold Nanoparticles. *Sci. Rep.* **2016**, *6*, 29230.

(23) Goodarzi, Z.; Maghrebi, M.; Zavareh, A. F.; Mokhtari-Hosseini, Z.-B.; Ebrahimi-hoseinzadeh, B.; Zarmi, A. H.; Barshan-tashnizi, M. Evaluation of Nicotine Sensor Based on Copper Nanoparticles and Carbon Nanotubes. *J. Nanostruct. Chem*. **2015**, *5*, 237–242.

(24) Fekry, A. M.; Azab, S. M.; Shehata, M.; Ameer, M. A. A Novel Electrochemical Nicotine Sensor Based on Cerium Nanoparticles with Anionic Surfactant. *RSC Adv*. **2015**, *5*, 51662–51671.

(25) Stočes, M.; Švancara, I. Electrochemical Behavior of Nicotine at Unmodified Carbon Paste Electrode and Its Determination in a Set of Refilling Liquids for Electronic Cigarettes. *Electroanalysis* **2014**, *26*, 2655–2663.

(26) Hecht, S. S.; Hochalter, J. B.; Villalta, P. W.; Murphy, S. E. 2'-Hydroxylation of Nicotine by Cytochrome P450 2A6 and Human Liver Microsomes: Formation of a Lung Carcinogen Precursor. *Proc. Natl. Acad. Sci. U. S. A.* **2010**, *97*, 12493−12497.

(27) Bloom, A. J.; Wang, P.-F.; Kharasch, E. D. Nicotine Oxidation by Genetic Variants of CYP2B6 and in Human Brain Microsomes. *Pharmacol Res Perspect.* **2019**, *7*, e00468.

(28) Yamazaki, H.; Inoue, K.; Hashimoto, M.; Shimada, T. Roles of CYP2A6 and CYP2B6 in Nicotine C-oxidation by Human Liver Microsomes. *Arch. Toxicol*. **1999**, *73*, 65-70.

(29) Dicke, K. E.; Skrlin, S. M.; Murphy, S. E. Nicotine and 4-(methylnitrosamino)-1-(3-pyridyl)-butanone Metabolism by Cytochrome P450 2B6. *Drug Metab. Dispos*. **2005**, *33*, 1760–1764.

(30) Lin, Y.; Bariya, M.; Nyein, H. Y. Y.; Kivimäki, L.; Uusitalo, S.; Jansson, E.; Ji, W.; Yuan, Z.; Happonen, T.; Liedert, C.; Hiltunen, J.; Fan, Z.; Javey, A. Porous Enzymatic Membrane for Nanotextured Glucose Sweat Sensors with High Stability toward Reliable Noninvasive Health Monitoring. *Adv. Funct. Mater*. **2019**, *29*, 1902521.

(31) Kamra, T.; Chaudhary, S.; Xu, C.; Montelius, L.; Schnadt, J.; Ye, L. Covalent Immobilization of Molecularly Imprinted Polymer Nanoparticles on a Gold Surface Using Carbodiimide Coupling for Chemical Sensing. *J. Colloid Interface Sci*. **2016**, *461*, 1-8.

(32) Fantuzzi, A.; Fairhead, M.; Gilardi, G. Direct Electrochemistry of Immobilized Human Cytochrome P450 2E1. *J. Am. Chem. Soc*. **2004**, *126*, 5040-5041.

(33) Alonso-Lomillo, M. A.; Yardimci, C.; Domínguez-Renedo, O.; Arcos-Martínez, M. J. CYP450 2B4 Covalently Attached to Carbon and Gold Screen Printed Electrodes by Diazonium Salt and Thiols Monolayers. *Anal. Chim. Acta* **2009**, *633*, 51-56.

(34) Peng, L.; Yang, X.; Zhang, Q.; Liu, S. Electrochemistry of Cytochrome P450 2B6 on Electrodes Modified with Zirconium Dioxide Nanoparticles and Platin Components. *Electroanalysis* **2008**, *20*, 803–807.

(35) Hatsukami, D. K.; Hertsgaard, L. A.; Vogel, R. I.; Jensen, J. A.; Murphy, S. E.; Hecht, S. S.; Carmella, S. G.; al'Absi, M.; Joseph, A. M.; Allen, S. S. Reduced Nicotine Content Cigarettes and Nicotine Patch. *Cancer Epidemiol., Biomarkers Prev*. **2013**, *22*, 1015-1024.

(36) Benowitz, N. L.; Dains, K. M.; Hall, S. M; Stewart, S.; Wilson, M.; Dempsey, D.; Jacob III, P. Smoking Behavior and Exposure to Tobacco Toxicants during 6 Months of Smoking Progressively Reduced Nicotine Content Cigarettes. *Cancer Epidemiol., Biomarkers Prev*. **2012**, *21*, 761-769.

(37) Bullen, C.; Howe, C.; Laugesen, M.; McRobbie, H.; Parag, V.; Williman, J.; Walker, N. Electronic Cigarettes for Smoking Cessation: a Randomised Controlled Trial. *Lancet* **2013**, *382*, 1629-1637.

(38) Benowitz, N. L.; Porchet, H.; Sheiner, L.; Jacob, P. Nicotine Absorption and Cardiovascular Effects with Smokeless Tobacco Use: Comparison with Cigarettes and Nicotine Gum. *Clin. Pharmacol. Ther.* **1988**, *44*, 23–28.

(39) Bernert, J. T.; Alexander, J. R.; Sosnoff, C. S.; McGuffey, J. E. Time Course of Nicotine and Cotinine Incorporation into Samples of Nonsmokers' Beard Hair Following a Single Dose of Nicotine Polacrilex. *J. Anal. Toxicol*. **2011**, *35*, 1-7.

(40) Yingst, J. M.; Foulds, J.; Veldheer, S.; Hrabovsky, S.; Trushin, N.; Eissenberg, T. T.; Williams, J.; Richie, J. P.; Nichols, T. T.; Wilson, S. J.; Hobkirk, A. L. Nicotine Absorption during Electronic Cigarette Use among Regular Users. *PLoS One* **2019**, *14*, e0220300.

(41) Berman, H. M.; Westbrook, J.; Feng, Z.; Gilliland, G.; Bhat, T. N.; Weissig, H.; Shindyalov, I. N.; Bourne, P. E. The Protein Data Bank. *Nucleic Acids Res*. **2000**, *28*, 235-242.

4.6 Appendix

Functionalization of electrodes to fabricate the nicotine sensor. Each sensor consists of a working electrode, a reference electrode, and a counter electrode, all prepared on a PET film. The sensors were initially patterned by photolithography technique with positive photoresist (Shipley Microposit S1818), and chromium (30 nm) and gold (50 nm) were evaporated subsequently with electron-beam to form a conductive three-electrode system. The working electrode was modified by growing gold nano-dendrites by immersing the electrode in a mixture solution of 50 mM chloroauric acid and 50 mM hydrochloric acid and applying an alternating potential via a Gamry Electrochemical Potentiostat (signal type: square wave; amplitude: 1 V; DC offset -1 V; signal frequency: 50 Hz; cycles: 1500). The electrodes were gently immersed in deionized water for ten seconds and left in room temperature for two hours. Afterward, the electrodes were immersed in 11-mercaptoundecanoic acid (MUA) solution (0.5 g MUA, 1 L ethanol) for 16 hours to allow self-assembled monolayers to form on top of the gold surface. Then, the electrodes were incubated in room temperature in a mixture of 1-ethyl-3-(3-dimethylaminopropyl)carbodiimide (EDC) and N-hydroxysuccinimide (NHS) solution (283 μL EDC, 62 mg NHS, 4 mL PBS) for 15 minutes. Afterward, the electrodes were incubated in a CYP2B6 enzyme solution for 1 hour before drop-casting the same solution on top of the working electrode (2.5 μL). The solution was prepared by mixing CYP2B6 (Sigma-Aldrich. 37.8 mg) in PBS (1 mL). The image of CYP2B6 in Figure 1 was created with www.rcsb.org.[41] The reference electrode was prepared by pasting silver/silver chloride ink onto the existing, evaporated gold electrode to provide a stable reference. The counter electrode was not modified further and remained as a simple gold electrode. The electrodes were left in room temperature for overnight for the enzyme and silver/silver chloride paste to stabilize prior to testing with a potentiostat.

Nicotine sensor's characterization and calibration in buffer solution. To characterize the functionalized working electrode, a commercial silver/silver chloride reference electrode and platinum wire were used to form a complete three-electrode electrochemical system in a PBS solution. CHI 1230C potentiostat (CH Instrument) was used for electrochemical measurements. Different concentrations of nicotine were subsequently added into the solution to obtain the corresponding CV and amperometric response. The sensor's response to temperature variation was performed by heating up the nicotine solution with a hotplate and measuring the solution's temperature with a thermometer. The amperometric response was captured once the solution reached the desired temperature. The sensor's response to pH was tested in McIlvaine buffer, which had an easily tunable range of pH. The

slight difference in baseline current was normalized between McIlvaine buffer with different pH. The interference test was performed by the subsequent addition of selected categories of common biomolecules in human bio-fluid. The concentration of each interferent was determined to be within the normal physiological range.

Nicotine sensor's characterization in sweat. The characterization of the on-body nicotine sensor in sweat solutions, shown in Figure 3, was conducted by first collecting sweat samples from volunteers. The amperometric response of the sensor was performed by directly connecting the functionalized working, reference, and counter electrodes to CHI 1230C potentiostat. The average value at each nicotine concentration in Figure 3b was used for plotting Figure 3c.

Sweat collection and nicotine concentration analysis. The sweat samples were collected via various methods. Volunteers were recruited from around the City of Berkeley. Sweat was generated by intense walking, cycling (Kettler E3 Upright Exercise Bike), or playing basketball. After perspiration began, a 200-μL centrifuge tube was used to collect sweat samples from the volunteers' foreheads. The volunteers cleaned their foreheads with gauze prior to each subsequent collection with a new centrifuge tube. Prior to testing the collected sweat samples, the nicotine sensor was characterized following the procedure described in the nicotine sensor's characterization section. Afterward, the collected sweat samples were evaluated with amperometry to convert the amperometric responses into nicotine concentrations. The institutional review board number approved at the University of California, Berkeley, is CPHS 2014-08-6636.

In situ sweat nicotine analysis. The volunteers engaged in cycling on a stationary ergometer at a biking (Kettler E3 Upright Exercise Bike) power of 100 W. The nicotine sensors, packaged in terms of the *s*-band, were mounted on top of the subjects' wrists over the entire duration of the cycling. The temperature calibration curve was used to convert the amperometric responses of the sensors operated at the skin temperatures of the subjects back to the current levels at room temperature, at which the sensors were characterized. The current levels were then converted to nicotine concentration using the calibration curves obtained prior to on-body exercise experiments. The raw data converted into nicotine concentration was further filtered (MATLAB Hampel Function and Smooth Function) on a personal computer.

Cigarette smoking. The smoking subjects smoked a cigarette right before engaging in physical exercise. A standard cigarette consists of approximately 13 mg of nicotine.[35-37]

Statistical procedures. During sensor characterization, statistical procedures were used. The sensors' sensitivities to nicotine are incorporated into a histogram plot in Figure 2e (10 sensors). The mean, median, and standard deviation are 4.4

nA/µM, 4.6 nA/µM, and 1.4 nA/µM, respectively. A representative sensor was chosen for figure 2d, with a sensitivity of 4.3 nA/µM. In subsequent sensor characterization in Figure 3 with sweat solution, the sensor is retested for confirmation purposes if its sensitivity shows a value that is more than a standard deviation away from the statistical mean.

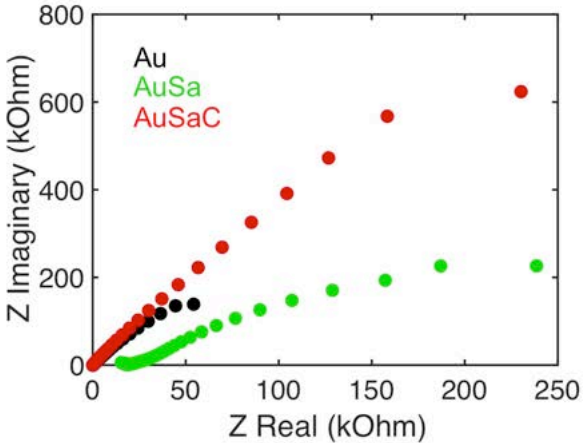

Figure S1. Electrochemical impedance spectroscopy of the gold electrode under various stages of modification. The increasing magnitude of impedance shows the addition of different modification layers onto the gold electrode. Bare gold (Au), gold and self-assembled monolayer (AuSa), gold and self-assembled monolayer and CYP2B6 enzyme (AuSaC) are shown, respectively. (Reprinted with permission from American Chemical Society).

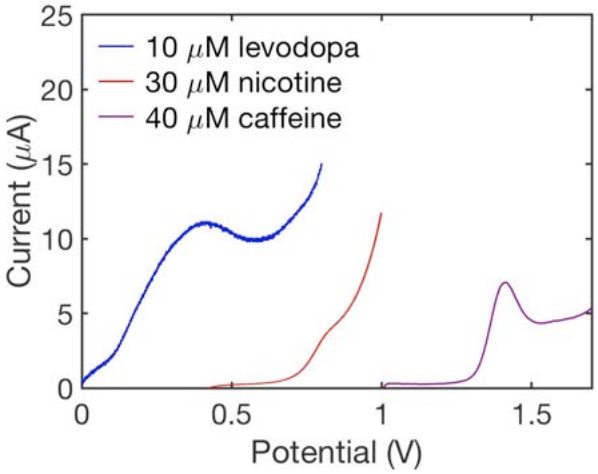

Figure S2. Oxidation peaks for selected xenobiotic molecules measured with cyclic voltammetry. The levodopa and caffeine data are from our previously published papers.[10,13] (Reprinted with permission from American Chemical Society).

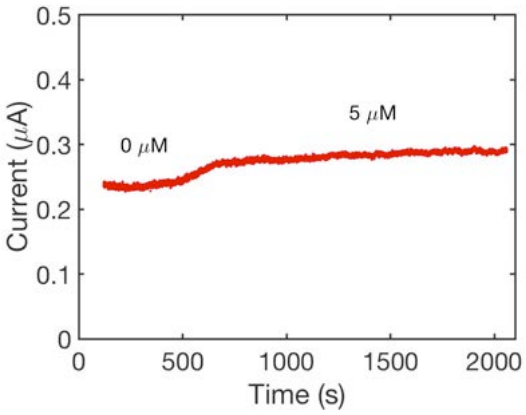

Figure S3. Long-term stability test of a functionalized working electrode. 5 µM nicotine is added at 400 sec. The drift corresponds to less than 0.16 µM/min. (Reprinted with permission from American Chemical Society).

Chapter 5 Conclusion

In conclusion, we have demonstrated skin-conforming wearable sensors capable of noninvasive, real-time and *in-situ* drug monitoring. The *s*-band compensates conventional drug monitoring techniques involving blood draws, urine collection or sweat collection by eliminating the requirement for separate sampling and analysis. The sweating profile measured by the *s*-band demonstrates its ability to inform users of their drug intake and metabolism. We also show that both iontophoresis and exercise induced sweat can serve as bases for drug detection.

In Chapter 2, the observed caffeine levels and metabolic trends are consistent with the physiological data reported in the literatures. Importantly, our work expands the realm of wearable sweat sensors towards drug monitoring, which is essential for clinical treatment of disease beyond diagnosis. The platform equipped with amenable DPV capabilities can be easily and broadly exploited to recognize a variety of drugs. Thus, the development of the drug monitoring *s*-band is an essential bridge for future applications in clinical pharmacology and precision medicine, such as therapeutic drug monitoring, drug abuse intervention and other aspects of the drug-related healthcare system.

In Chapter 3, we demonstrated the performance of a wearable sweat band for monitoring the metabolic behavior of levodopa, the standard medication prescribed to Parkinson's disease patients. The levodopa *s*-band integrates various material innovations and enables us to gain fundamental insights into the pharmacokinetic behavior of levodopa noninvasively.

In Chapter 4, the *s*-band overcomes the shortcomings of other commercial tobacco detectors that are limited by their lack of mobility and inability for continuous measurements. From the society's point of view, the *s*-band provides the general population an excellent device to monitor secondhand smoke and allows for effective policymaking related to smoke prevention. We envision that the nicotine *s*-band's long-term monitoring capability and its application geared toward the general public will significantly expand the realm of wearable sensing technologies and chart new territories for biomedical discoveries. Further, the longitudinal and cross sectional studies enabled through the nicotine *s*-band will provide us with profound insight into various chronic and underlying pathological conditions that can be explored for preventive care and personalized medication.

Our drug monitoring wearable platform, with other existing networks of wearable sweat sensors, can enable unprecedented studies on pharmacokinetics to understand the interplays between drugs and wide-ranging biomolecules in the human body. In tandem with big data and artificial intelligence techniques, we envision that these systems of biomedical sensors can provide profound insight

into the intrinsically complex and inextricably linked human physiology, pathology and neuropsychology related to drugs.